

# **Special Topics in Particle Physics**

## **Secondary Cosmic Rays**

**Helga Dénés 2024 S1 Yachay Tech**

[hdenes@yachaytech.edu.ec](mailto:hdenes@yachaytech.edu.ec)

# Secondary cosmic rays

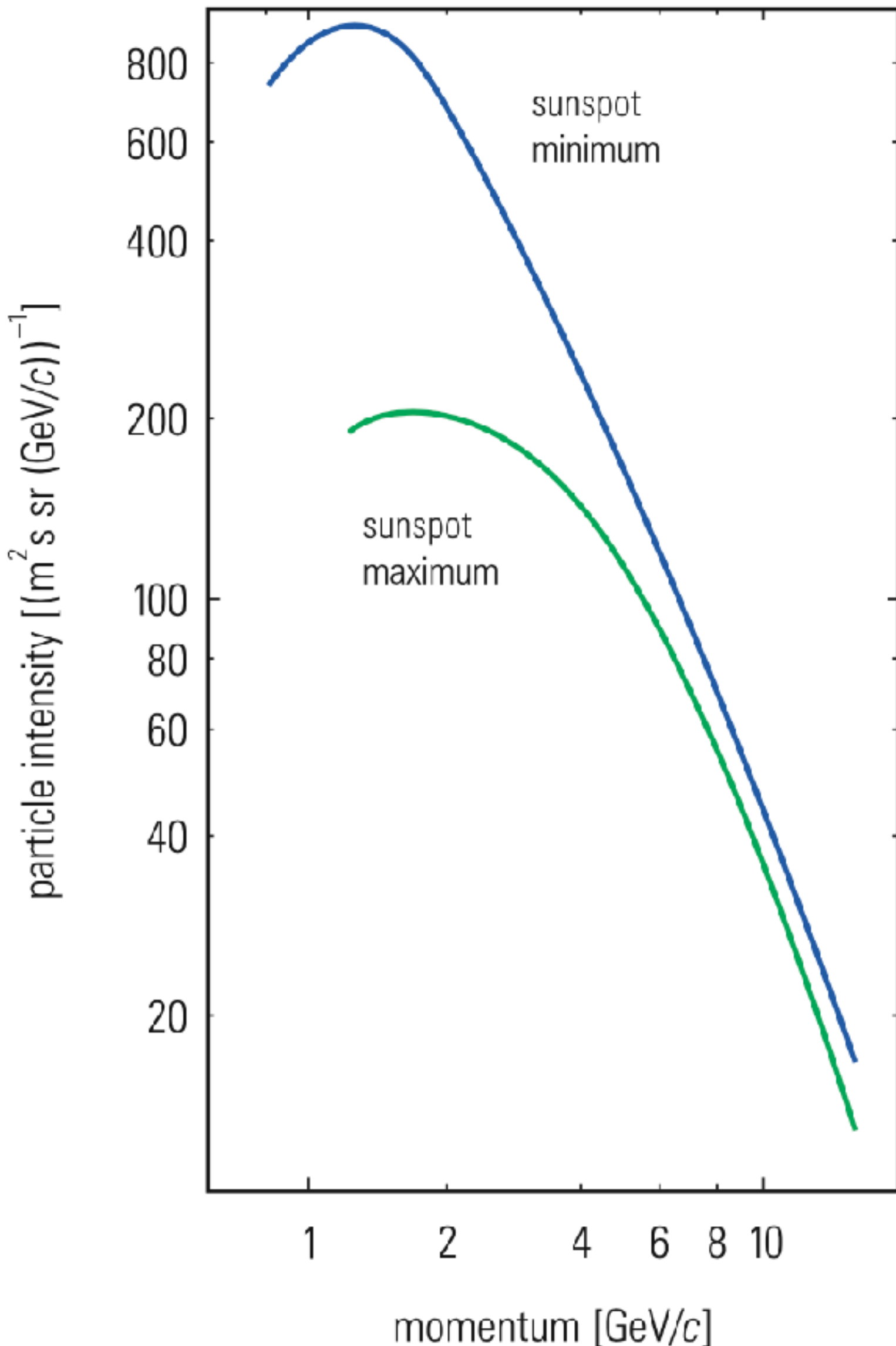
**Fig. 7.1** Modulation of the primary spectrum by the 11-year cycle of the Sun

For the purpose of astroparticle physics the influence of the Sun's and the Earth's magnetic field is a perturbation, which complicates a search for the sources of cosmic rays.

The **solar activity produces an additional magnetic field**, which prevents part of galactic cosmic rays from reaching Earth.

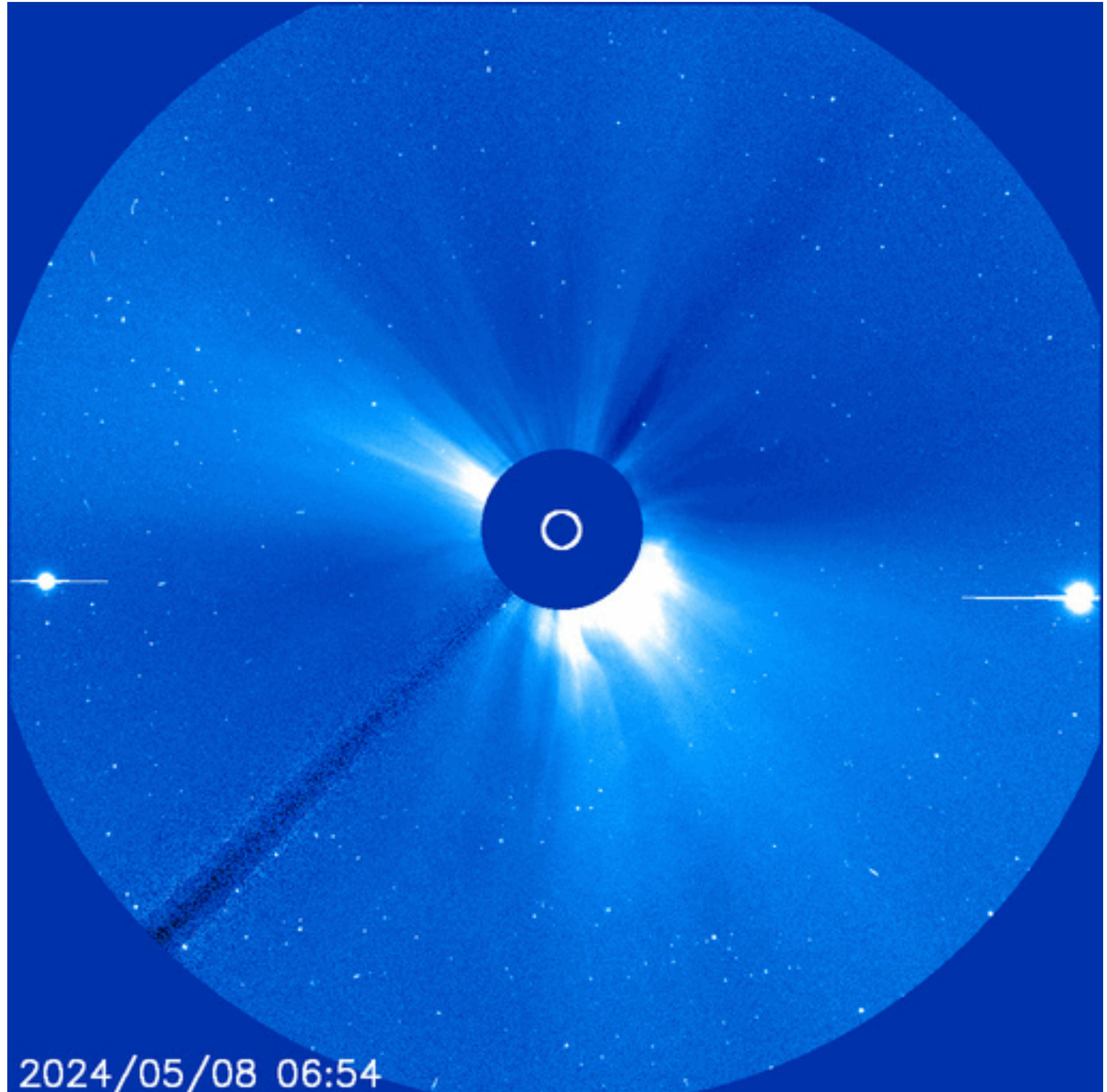
Figure 7.1, however, shows that **the influence of the Sun is limited to primary particles with energies below 10GeV**.

The **flux of low-energy primary cosmic-ray particles is anti-correlated to the solar activity**.



# Secondary cosmic rays

Recent solar activity: 6 CMEs produced on 8-9 May 2024 → disturbance in Earth's magnetosphere + intense aurora activity. Auroras were observed at such low latitude as the Canary Islands and Hawaii.



# Secondary cosmic rays

On the other hand, the **solar wind**, whose magnetic field modulates primary cosmic rays, is a particle stream in itself, which can be measured at Earth.

The particles constituting the **solar wind** (predominantly protons and electrons) are of **low energy** (MeV region). These particles are **captured to a large extent by the Earth's magnetic field** in the **Van Allen belts** or they are absorbed in the upper layers of the Earth's atmosphere (see Fig. 1.10).

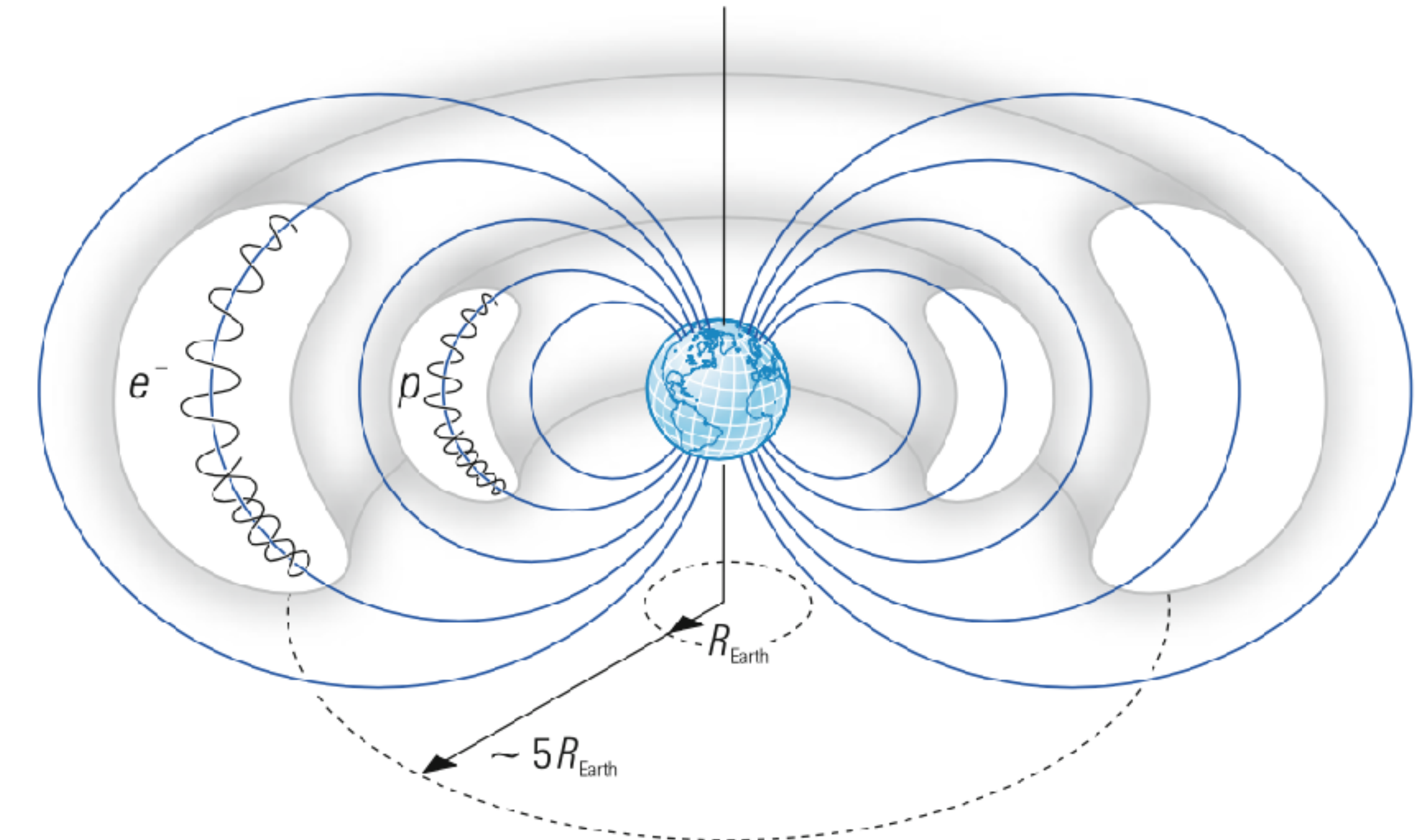


**Fig. 1.10** Van Allen radiation belts

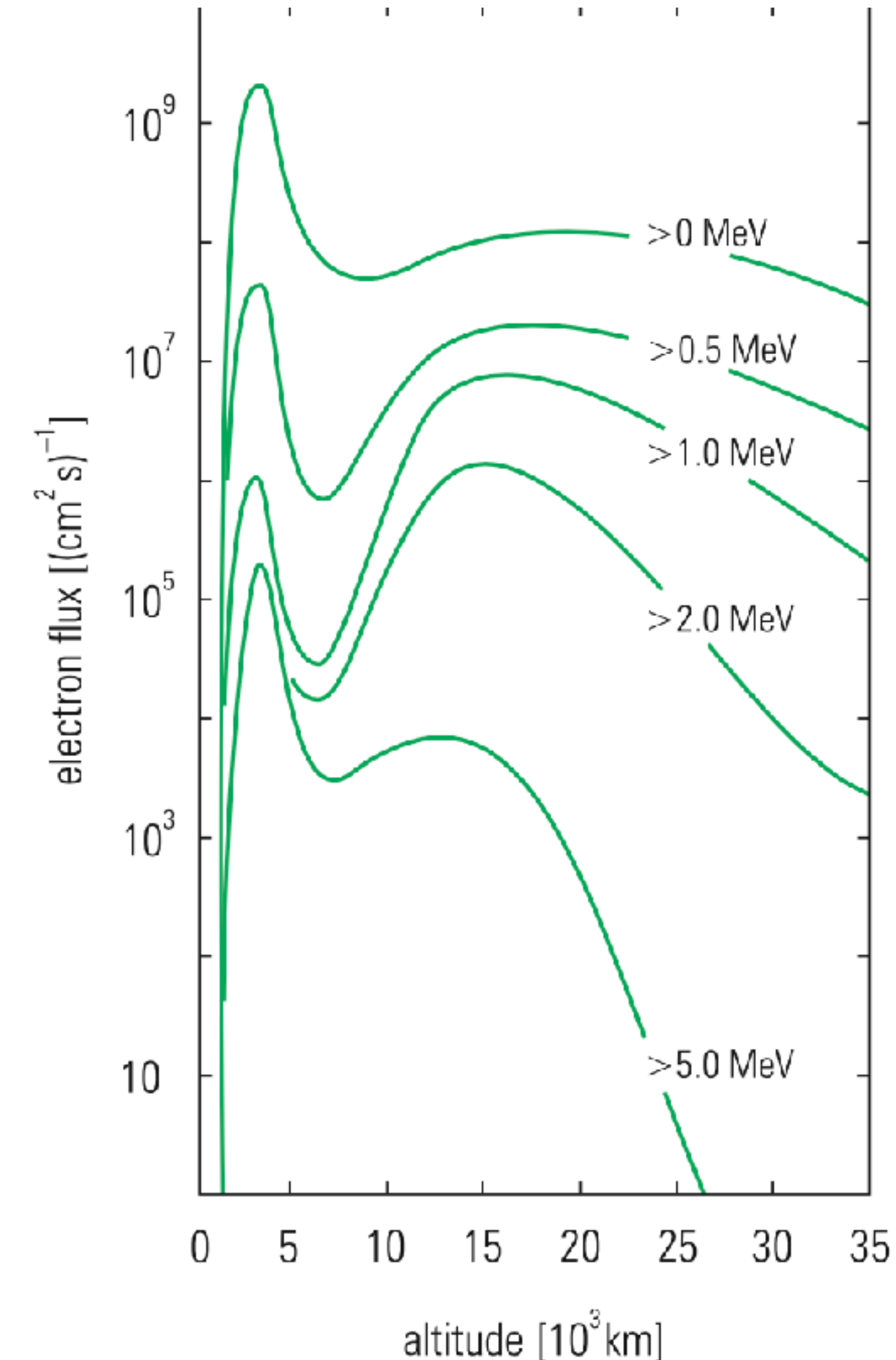
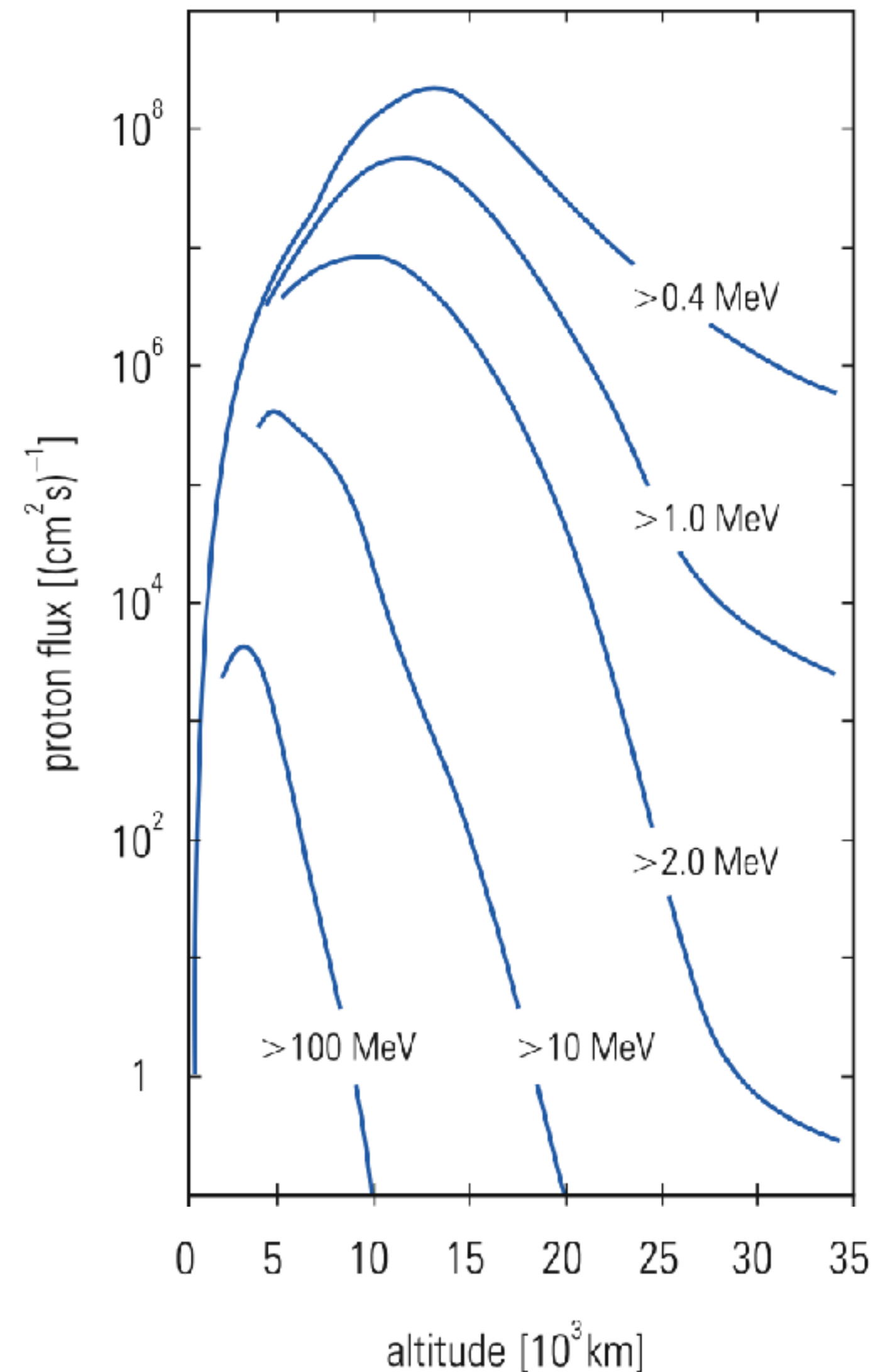
# Secondary cosmic rays

Figure 7.2 shows the **flux densities of protons and electrons in the Van Allen belts.**

The **proton belt** extends over altitudes from **2000 to 15 000 km**. It contains particles with intensities up to  $10^8/(\text{cm}^2 \text{ s})$  and energies up to **1 GeV**.

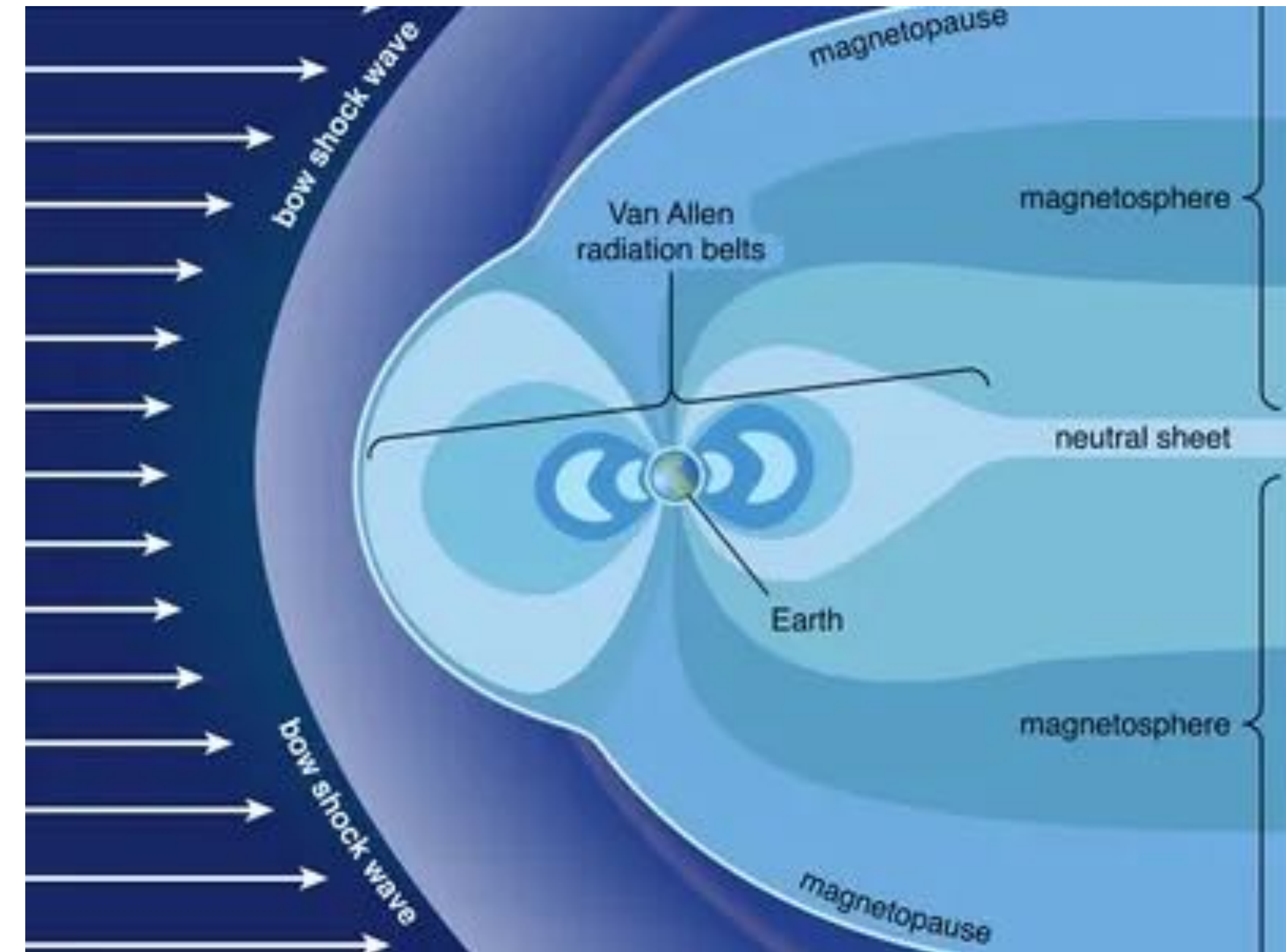
The **electron belt** consists of **two parts**. The **inner electron belt** with flux densities of up to  $10^9$  particles per  $\text{cm}^2$  and  $\text{s}$  is at an altitude of approximately **3000 km**, while the **outer belt** extends from about **15000 to 25000 km**.

**Fig. 7.2** Flux densities of protons and electrons in the radiation belts of the Earth



# Secondary cosmic rays

The inner part of the radiation belts is symmetrically distributed around the Earth while the outer part is subject to the influence of the solar wind and consequently deformed by it.



# Propagation in the atmosphere

Primary cosmic rays are strongly modified by interactions with atomic nuclei in the atmospheric air.

The column density of the atmosphere amounts to approximately  $1000 \text{ g/cm}^2$ , corresponding to an atmospheric pressure of about 1000 hPa.

The residual atmosphere for flight altitudes of scientific balloons ( $\approx 35\text{--}40 \text{ km}$ ) corresponds to approximately several  $\text{g/cm}^2$ . For inclined directions the thickness of the atmosphere increases strongly (approximately like  $1/\cos \theta$ , with  $\theta$  — zenith angle).

For the interaction behaviour of primary cosmic rays the thickness of the atmosphere in units of the characteristic interaction lengths for the relevant particles species is important. The ***radiation length for photons and electrons*** in air is  $X_0 = 36.66 \text{ g/cm}^2$ . The atmosphere therefore corresponds to a depth of 27 radiation lengths.

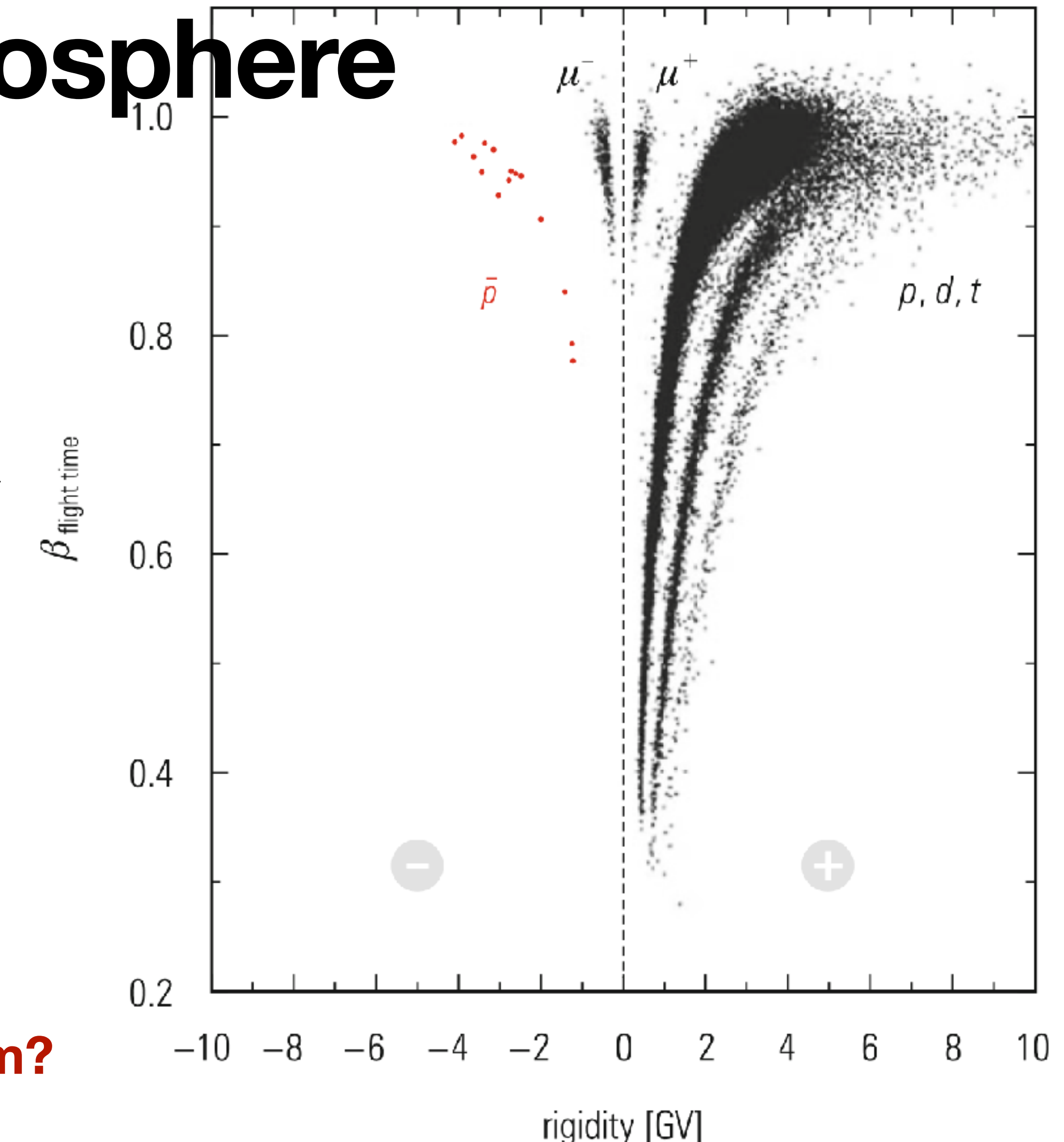
The relevant ***interaction length*** for hadrons in air is  $\lambda = 90.0 \text{ g/cm}^2$ , corresponding to 11 interaction lengths per atmosphere.

This means that ***practically not a single particle of original primary cosmic rays arrives at sea level***. Already at altitudes of 15–20 km primary cosmic rays interact with atomic nuclei of the air and initiate—depending on energy and particle species—***electromagnetic and/or hadronic cascades***.

# Propagation in the atmosphere

The **momentum spectrum of the singly charged component of primary cosmic rays at the top of the atmosphere** is shown in Fig. 7.3.

In this diagram the **particle velocity**  $\beta = v/c$  is shown as a **function of momentum** (more precisely the **rigidity** is plotted, which is the momentum divided by the charge of the primary particle  $p/Z$ ; since in this case  $Z = 1$ , momentum and rigidity are identical).



**Which particles are included on the diagram?**

**Fig. 7.3** Identification of singly charged particles in primary cosmic rays, measured at flight altitudes of a balloon at a residual atmosphere of  $5 \text{ g/cm}^2$  [110]

# Propagation in the atmosphere

Clearly visible are the bands of **hydrogen isotopes** as well as the low flux of **primary antiprotons**.

Even at these altitudes **several muons have been produced via pion decays**. Since muon and pion mass are very close, it is impossible to separate them out in this scatter diagram.

Also **relativistic electrons and positrons** would populate the bands labeled  $\mu^+$  and  $\mu^-$ .

One generally assumes that the **measured antiprotons are not of primordial origin**, but are rather **produced by interactions in interstellar or interplanetary space or even in the residual atmosphere above the balloon**.

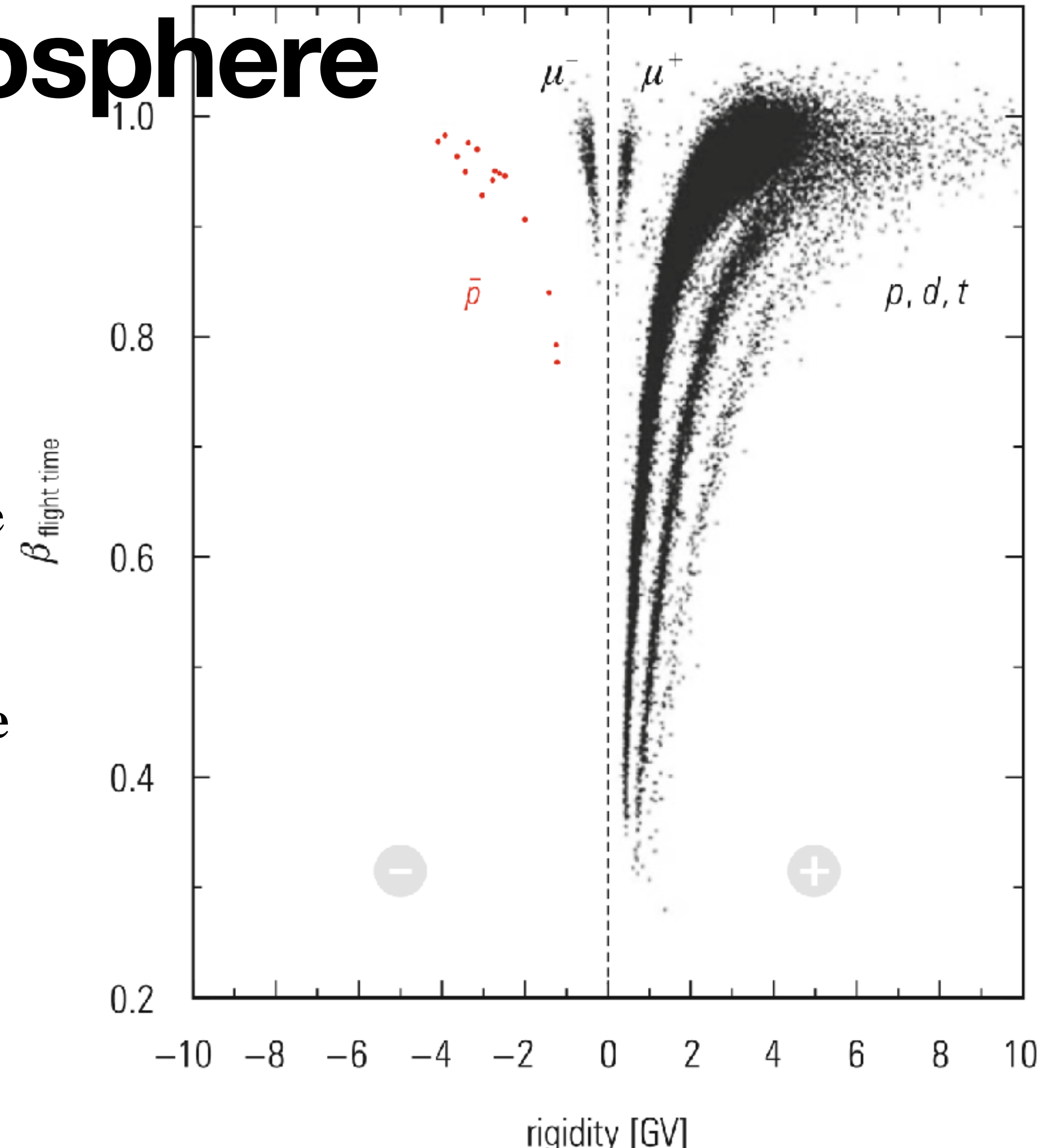


**Fig. 7.3** Identification of singly charged particles in primary cosmic rays, measured at flight altitudes of a balloon at a residual atmosphere of  $5 \text{ g/cm}^2$  [110]

**Fig. 7.4** Transformation of primary cosmic rays in the atmosphere

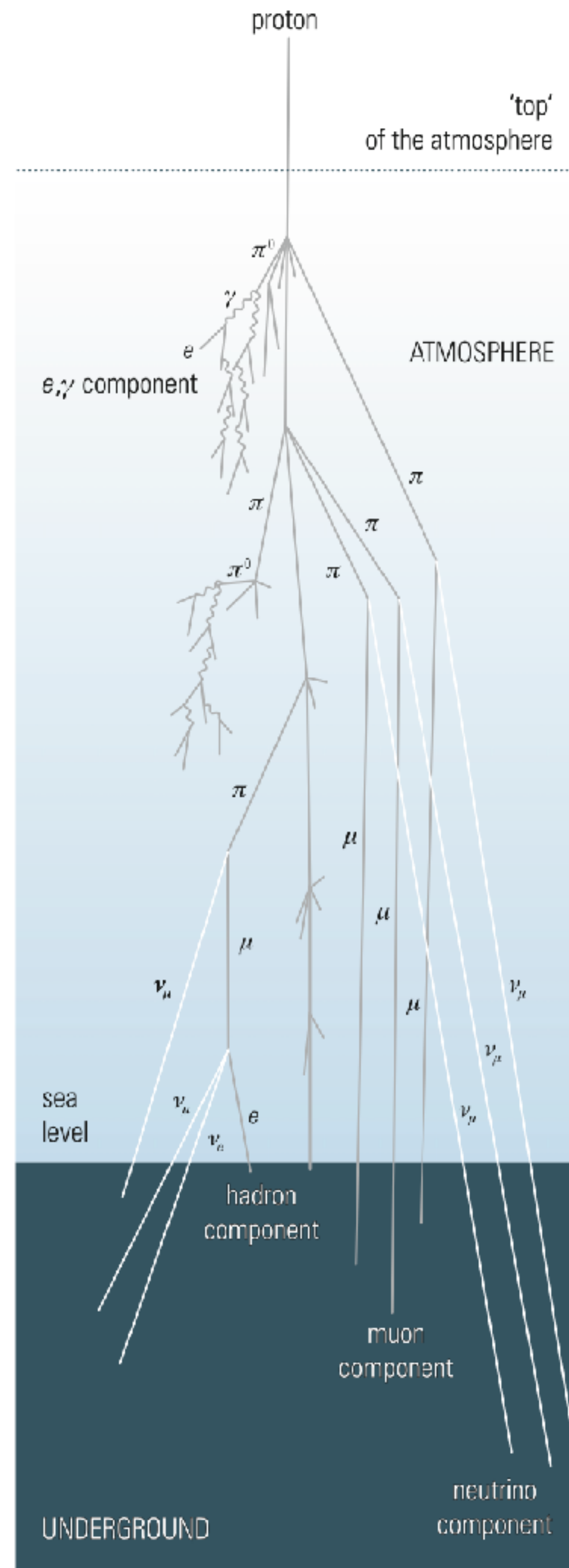
# Propagation in the atmosphere

The transformation of primary cosmic rays in the atmosphere is presented in Fig. 7.4.

Protons with approximately **85%** probability constitute the **largest fraction of primary cosmic rays**. Since the interaction length for hadrons is  $90 \text{ g/cm}^2$ , primary protons **initiate a hadron cascade** already in their first interaction approximately at an altitude corresponding to the **100-mbar layer**.

The **secondary particles** most copiously produced **are pions**.

**Kaons**, on the other hand, are only produced with a **probability of 10–15%** compared to pions.



# Propagation in the atmosphere

Figure 7.5 shows the  $K/\pi$  ratio as it is measured in strong interactions.

For center-of-mass energies  $\sqrt{s}$  in the range from **20 GeV to 300 GeV** the  $K/\pi$  ratio is **more or less constant**.

To translate center-of-mass energies to laboratory energies one finds that 300 GeV in the center of mass corresponds to **45 TeV in the laboratory system**.

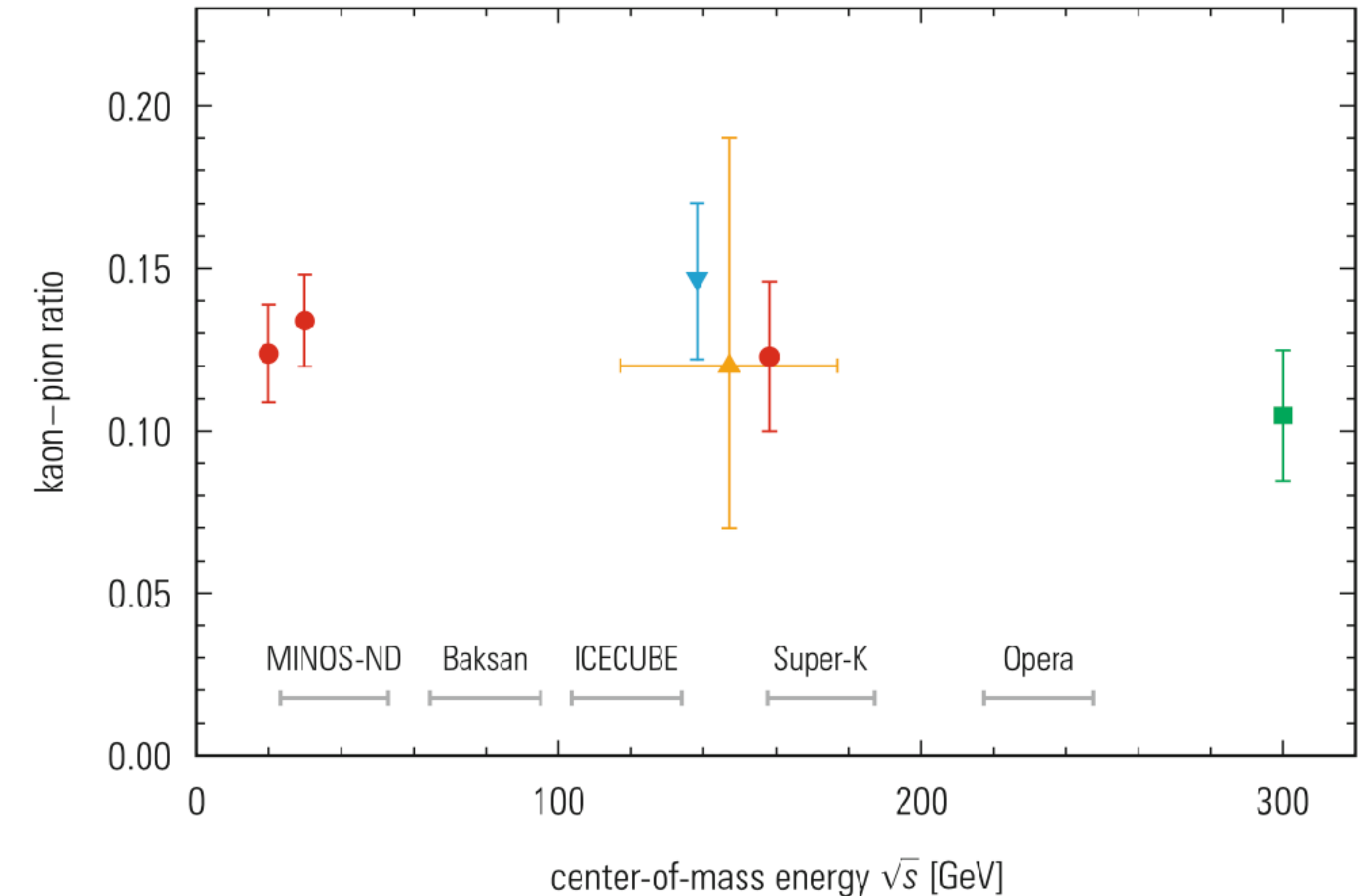


**Fig. 7.5** Kaon–pion ratio as obtained in strong interactions. Compilation of results of different experiments for the measurement of the  $K/\pi$  ratio. (In the legend ‘Super-K’ stands for Super-Kamiokande.) The data are from proton–proton interactions and collisions of heavy ions. The typical center-of-mass energies of the various experiments are converted to laboratory energies as indicated above the horizontal axis [111]

# Propagation in the atmosphere

Neutral pions initiate via their decay ( $\pi^0 \rightarrow \gamma + \gamma$ ) **electromagnetic cascades**, whose development is characterized by the **shorter radiation length** ( $X_0 \approx \frac{1}{3} \lambda$  in air).

This shower component is absorbed relatively easily and is therefore also named a **soft component**.

Charged **pions and kaons can either initiate further interactions or decay**.

The competition between decay and interaction probability is a function of energy. For the same Lorentz factor charged pions ( $\tau = 26$  ns) have a smaller decay probability compared to charged kaons ( $\tau = 12.4$  ns).

The leptonic decays of pions and kaons produce the penetrating **muon and neutrino components**

$$\pi^+ \rightarrow \mu^+ + \nu_\mu, \pi^- \rightarrow \mu^- + \bar{\nu}_\mu$$

**Draw the Feynman diagram!**

$$K^+ \rightarrow \mu^+ + \nu_\mu, K^- \rightarrow \mu^- + \bar{\nu}_\mu.$$

Muons can also decay and contribute via their decay **electrons to the soft component and neutrinos to the neutrino component**  $\mu^+ \rightarrow e^+ + \nu_e + \bar{\nu}_\mu, \mu^- \rightarrow e^- + \bar{\nu}_e + \nu_\mu$ .

**Draw the Feynman diagram!**

# Propagation in the atmosphere

The energy loss of **relativistic muons not decaying** in the atmosphere is low ( $\approx 1.8$  GeV). They **constitute with 80% of all charged particles** the largest fraction of secondary particles **at sea level**.

**Some secondary mesons and baryons can also survive down to sea level.** Most of the **low-energy charged hadrons observed at sea level are locally produced.** The total fraction of hadrons at ground level, however, is very small.

Apart from their longitudinal development electromagnetic and hadronic cascades **also spread out laterally in the atmosphere.**

The **lateral size of an electromagnetic cascade** is caused by **multiple scattering** of electrons and positrons, while in **hadronic cascades the transverse momenta** at production of secondary particles are responsible for the lateral width of the cascade.

# Propagation in the atmosphere

Figures 7.6, 7.7, and 7.8 show a comparison of the **shower development of 1-TeV photons, 1-TeV protons, and 1-TeV iron nuclei in the atmosphere**. It is clearly visible that transverse momenta of secondary particles fan out the hadron cascades.

**Fig. 7.6** Simulation of a 1-TeV photon in the atmosphere. Scale: vertical about 30 km, lateral 10 km [84]

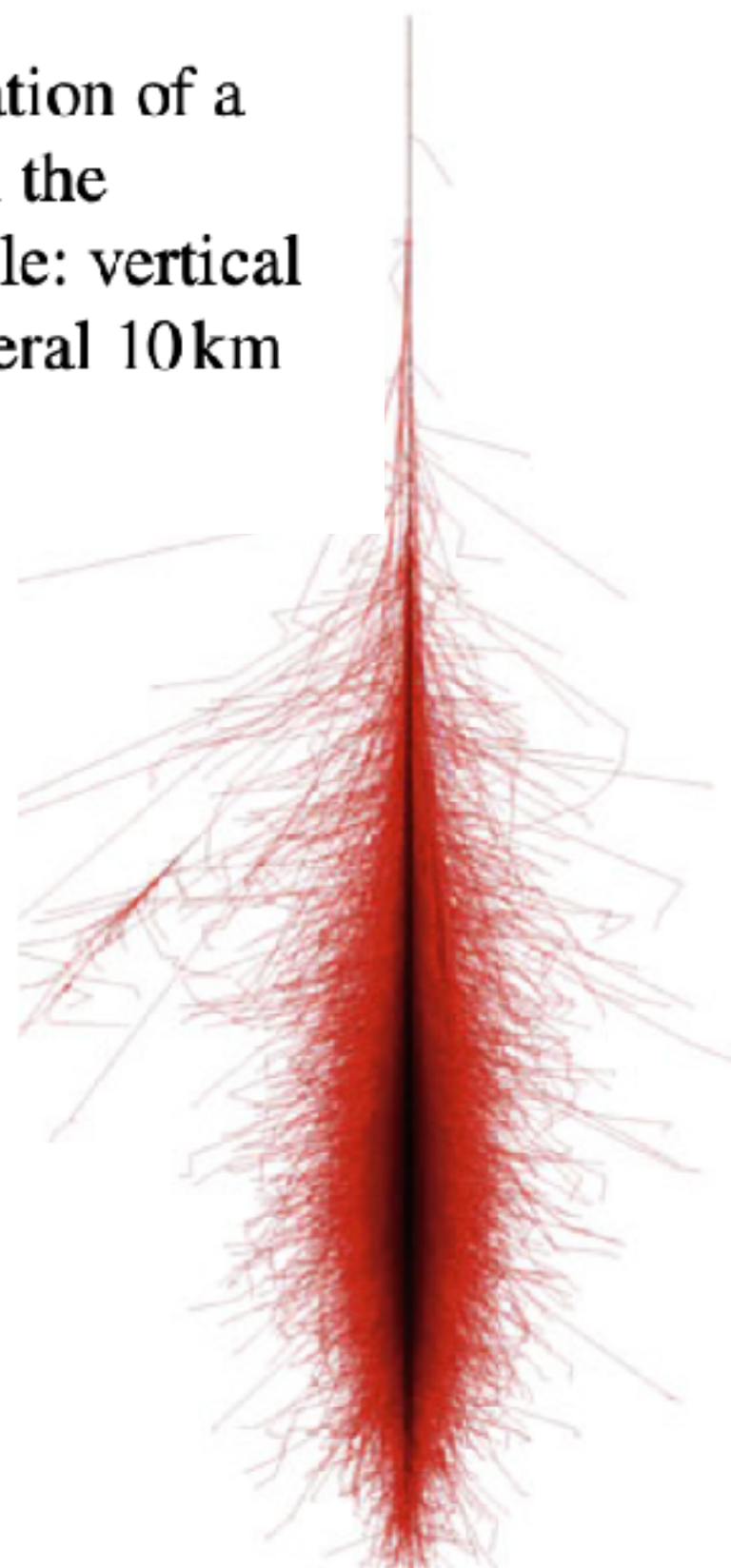


**Fig. 7.7** Simulation of a 1-TeV proton in the atmosphere. Scale: vertical about 30 km, lateral 10 km [84]

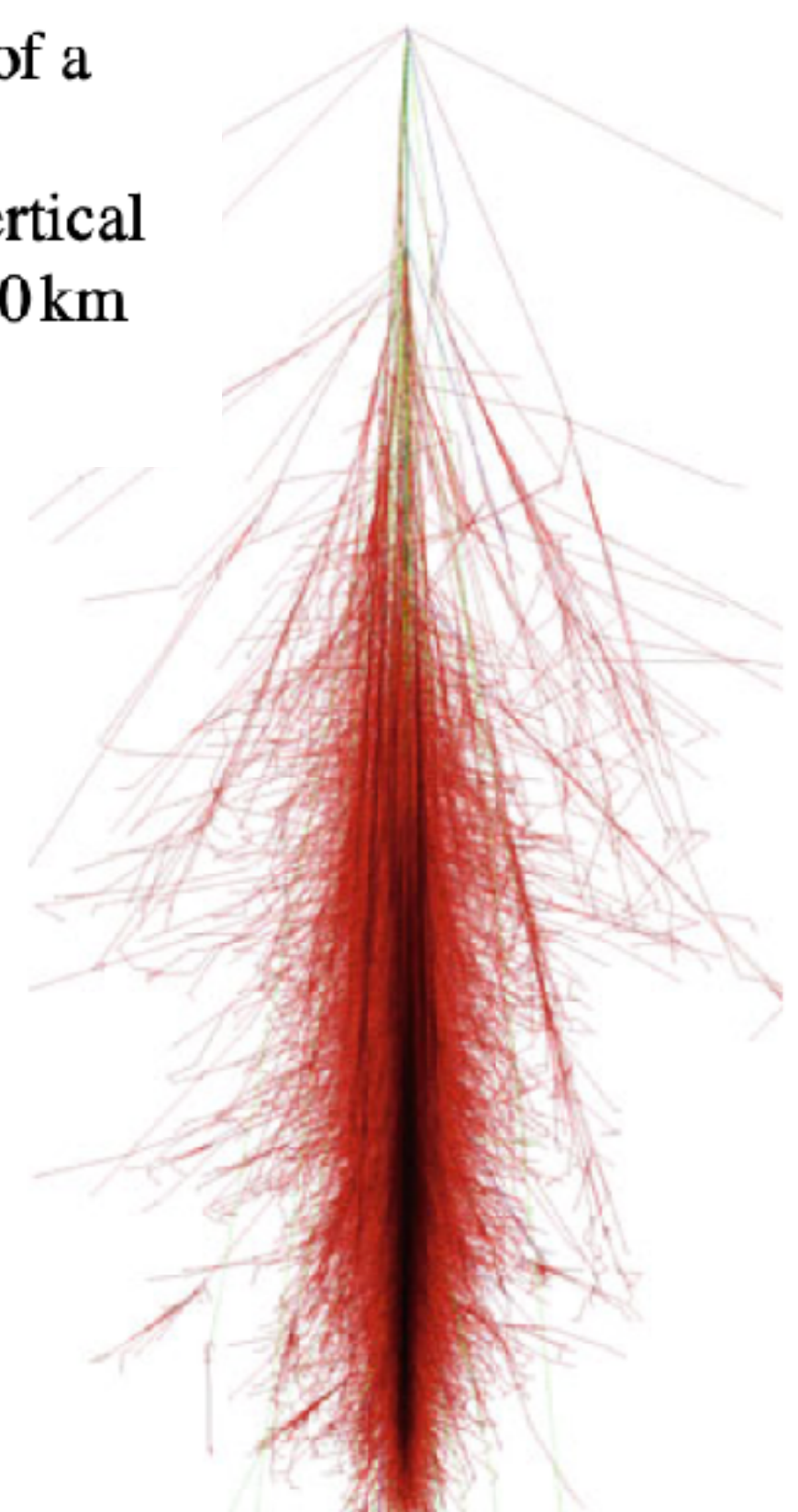
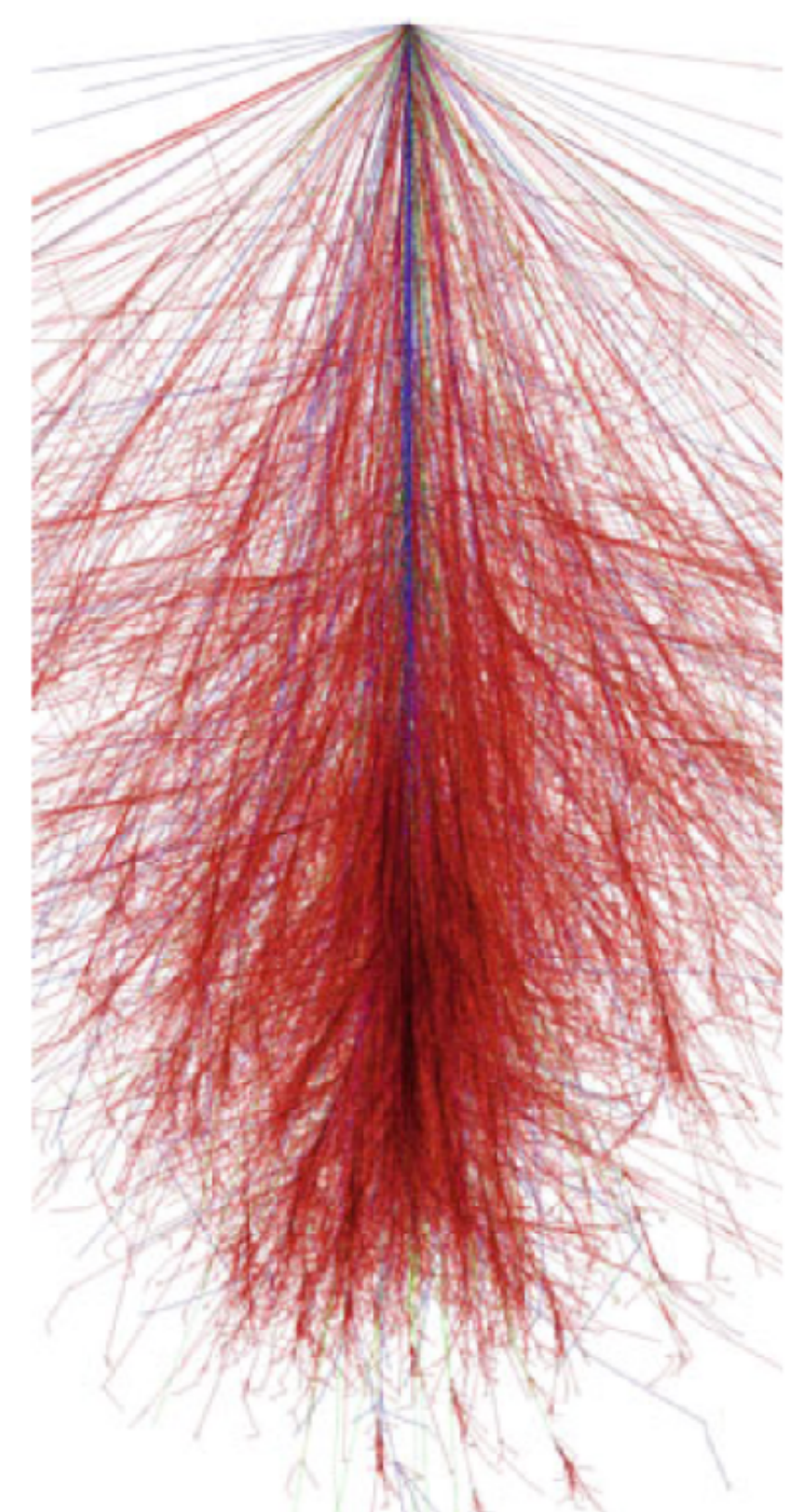


**Fig. 7.8** Simulation of an iron nucleus of 1 TeV in the atmosphere. Scale: vertical about 30 km, lateral 10 km [84]



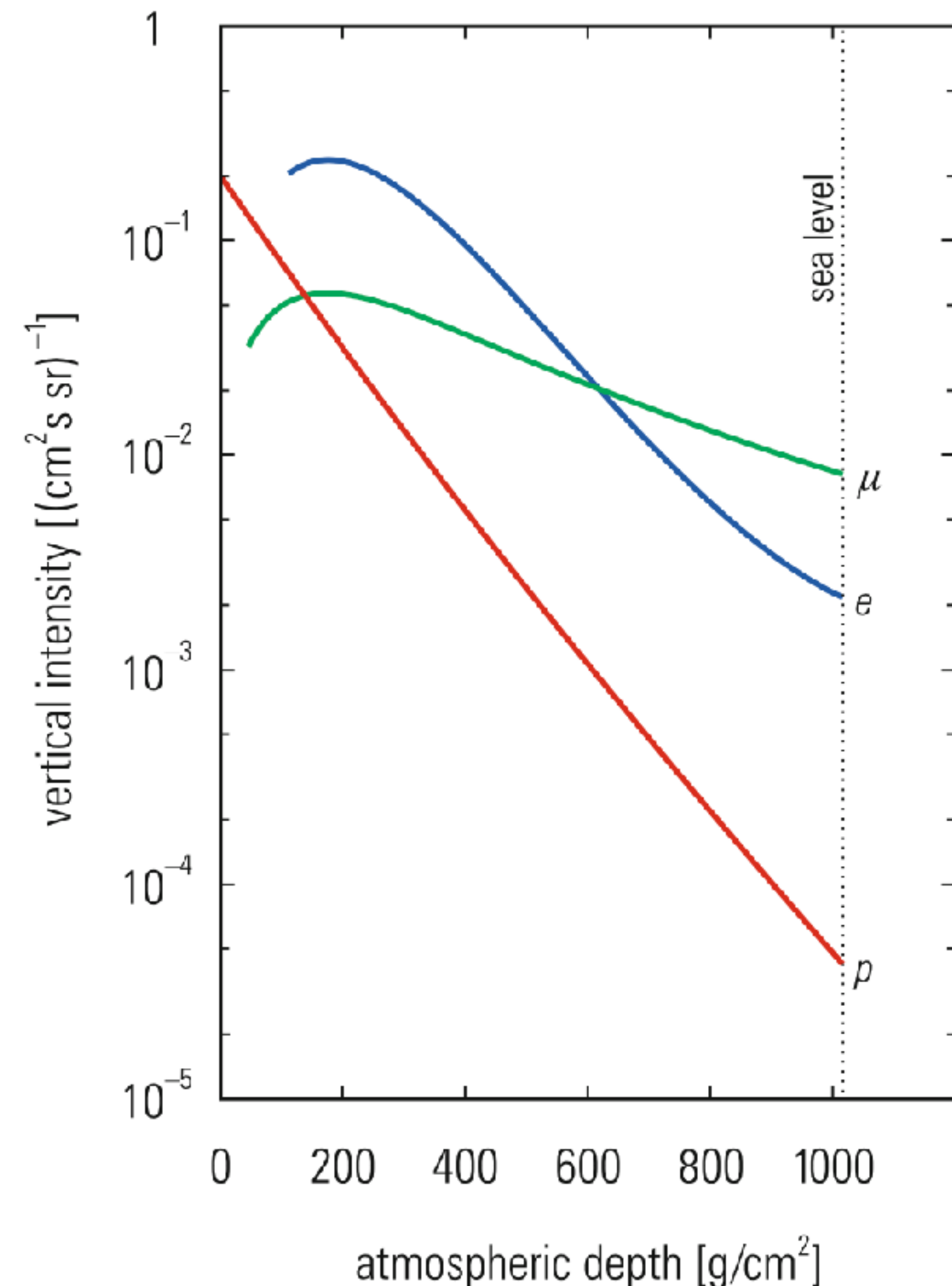
# Propagation in the atmosphere

**Fig. 7.9** Particle composition in the atmosphere as a function of atmospheric depth [112]

The **intensity of protons, electrons, and muons** of all energies **as a function of the altitude in the atmosphere** is plotted in Fig. 7.9. The absorption of protons can be approximately described by an exponential function.

The **electrons and positrons** produced through  $\pi^0$  decay with subsequent pair production reach a **maximum** intensity at an altitude of approximately **15km** and soon after are relatively quickly absorbed while, in contrast, the **flux of muons** is **attenuated only relatively weakly**.

Because of the steepness of the energy spectra the particle intensities are of course **dominated by low-energy particles**. These low-energy particles, however, are mostly of **secondary origin**.



# Propagation in the atmosphere

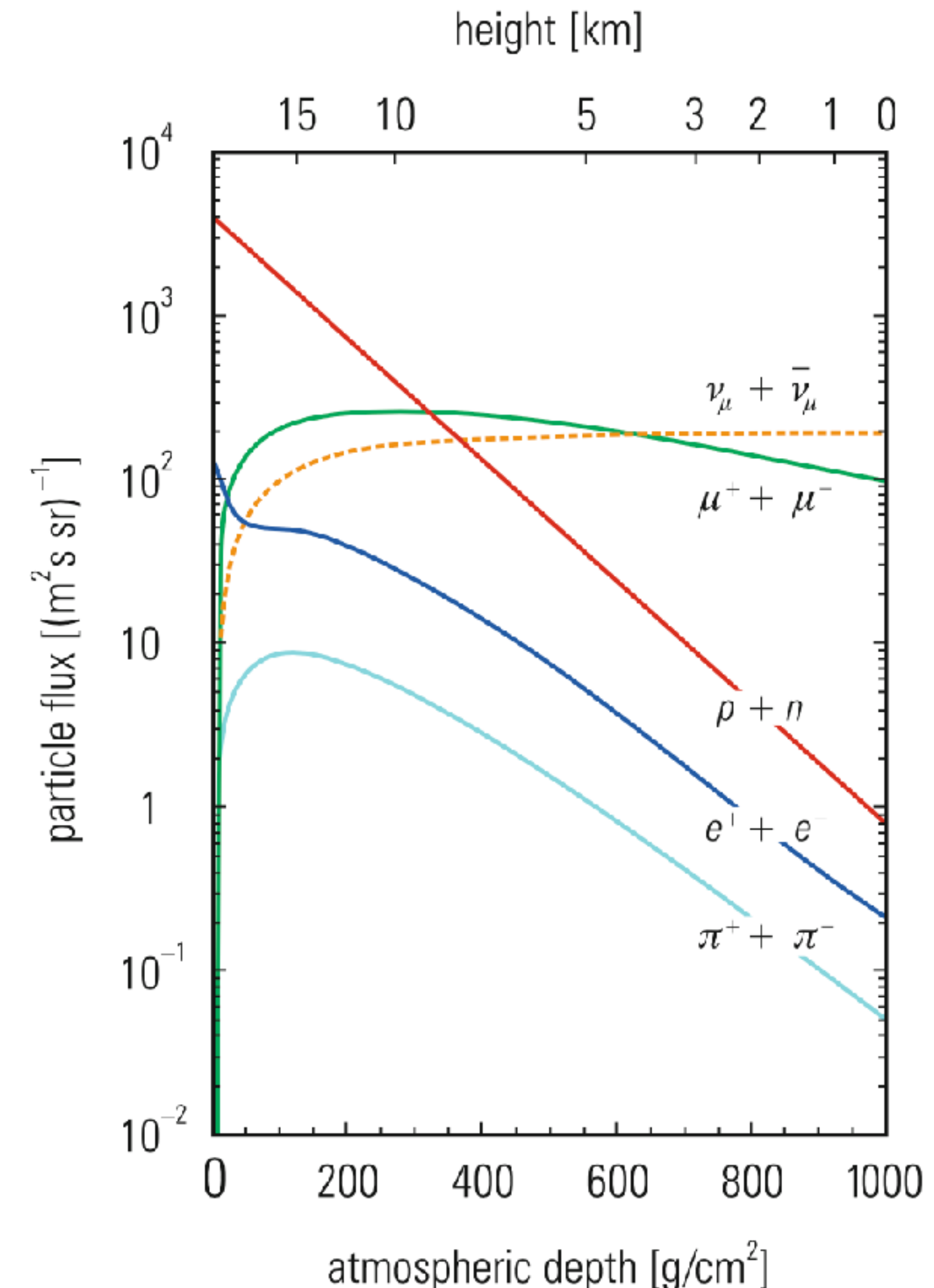
**Fig. 7.10** Particle composition in the atmosphere as function of the atmospheric depth for particles with energies  $>1\text{ GeV}$  [112]

If **only particles with energies in excess of 1 GeV** are counted, a different picture emerges (Fig. 7.10).

**Nucleons** (protons and neutrons) with the initial high energies **dominate** over all other particle species down **to altitudes of 9km**, where **muons take over**.

Because of the low interaction probability of **neutrinos** these particles are practically **not at all absorbed** in the atmosphere. Their **flux increases** monotonically **because additional neutrinos are produced** by particle decays.

Since the energy spectrum of primary particles is relatively steep, the energy distribution of secondaries also has to reflect this property.



# Cosmic rays at sea level

A measurement of charged particles at **sea level** clearly shows that, apart from **some protons**, **muons are the dominant component** (Fig. 7.11).

**Approximately 80%** of the charged component of secondary cosmic rays at sea level are muons.

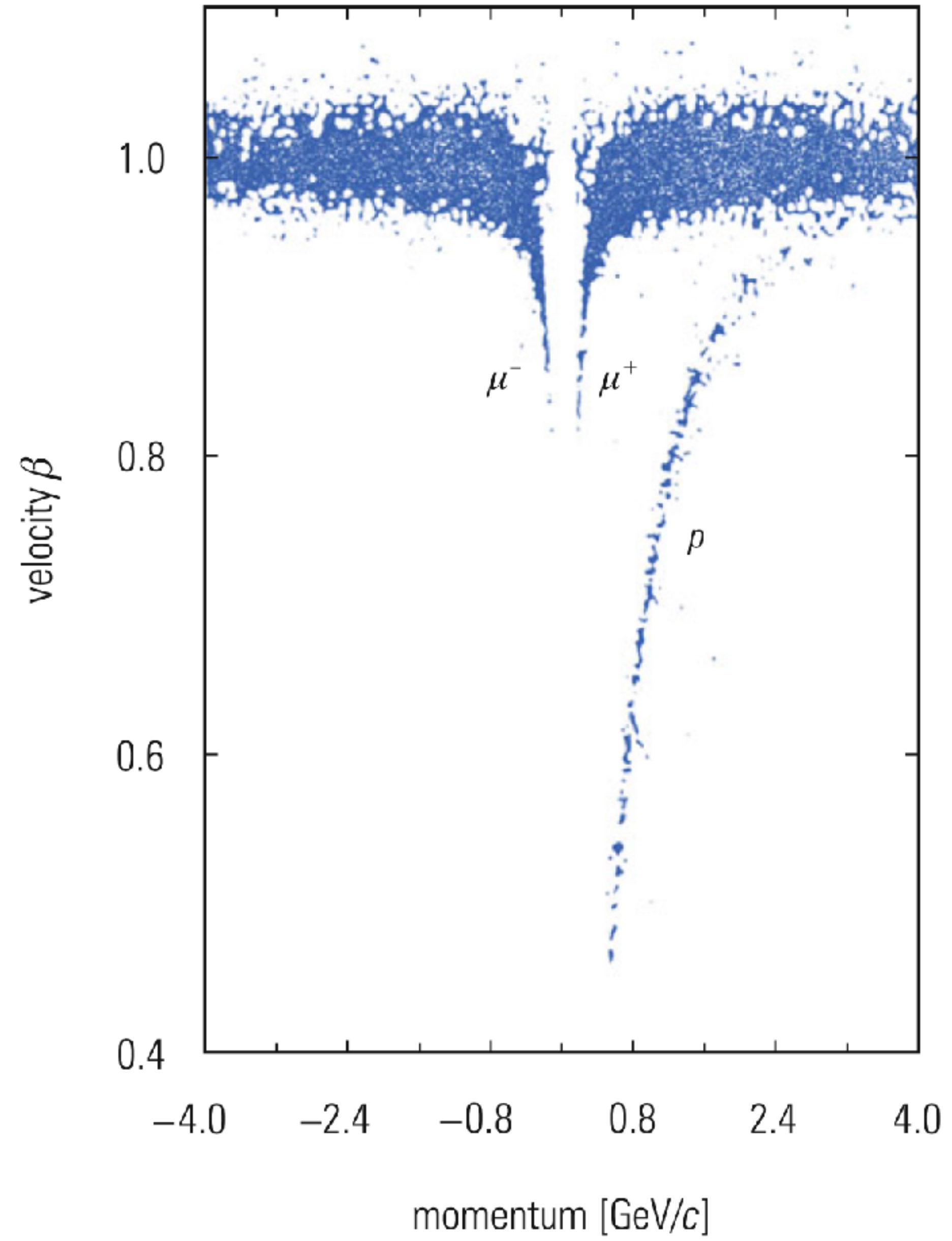


**Fig. 7.11** Measurement and identification of charged particles at sea level [113]

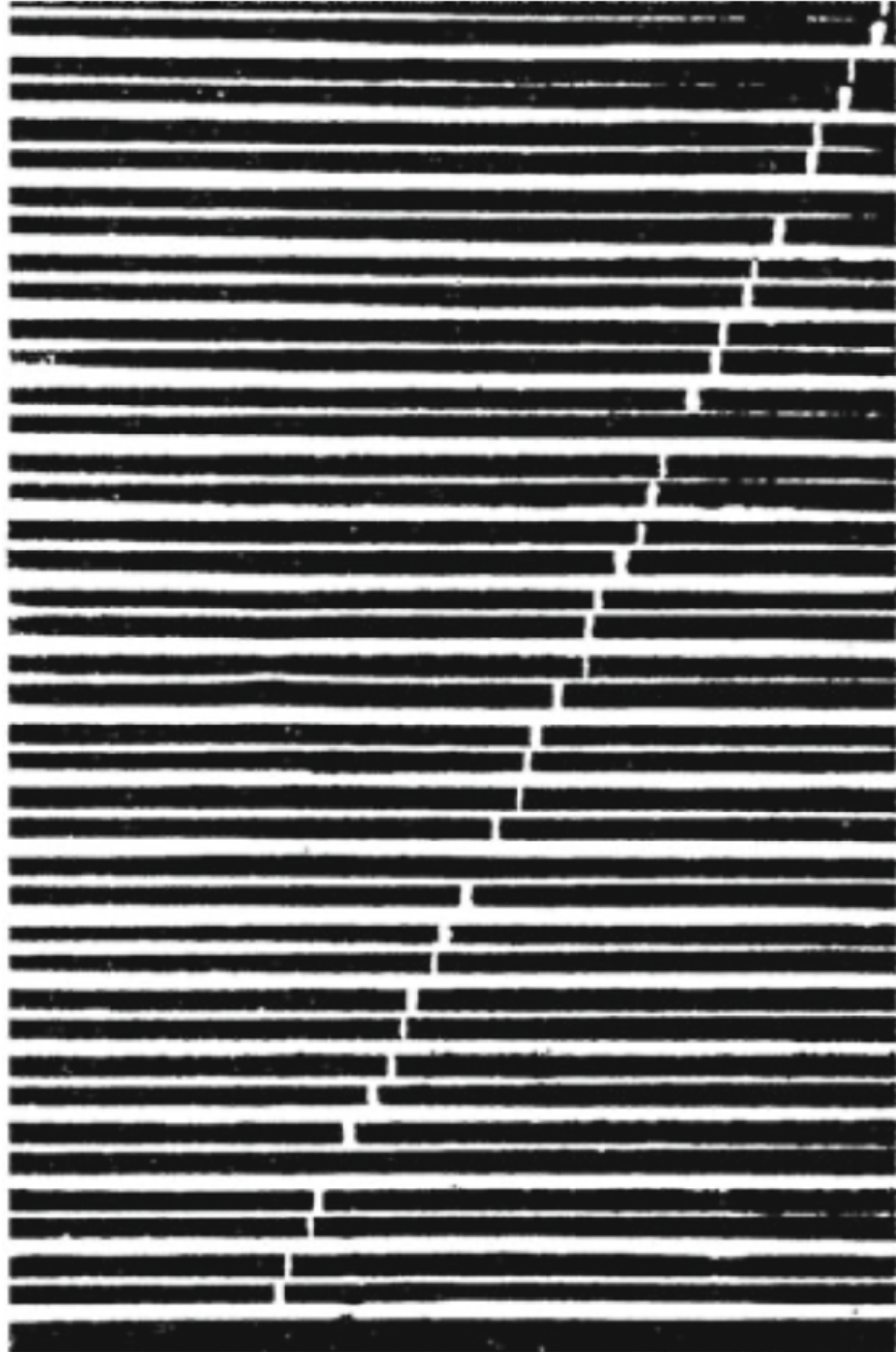
# Cosmic rays at sea level

**Fig. 7.12** Cosmic-ray muon,  
recorded in a multiplate  
spark chamber, 1957 [114]

Figure 7.12 shows the **track of a cosmic-ray muon** in a historical optical multiplate spark chamber.

The muon flux at sea level through a horizontal area amounts to **roughly one particle per  $\text{cm}^2$  per minute**.

These muons originate **predominantly from pion decays**, since pions as lightest mesons are produced in large numbers in hadron cascades.



# Cosmic rays at sea level

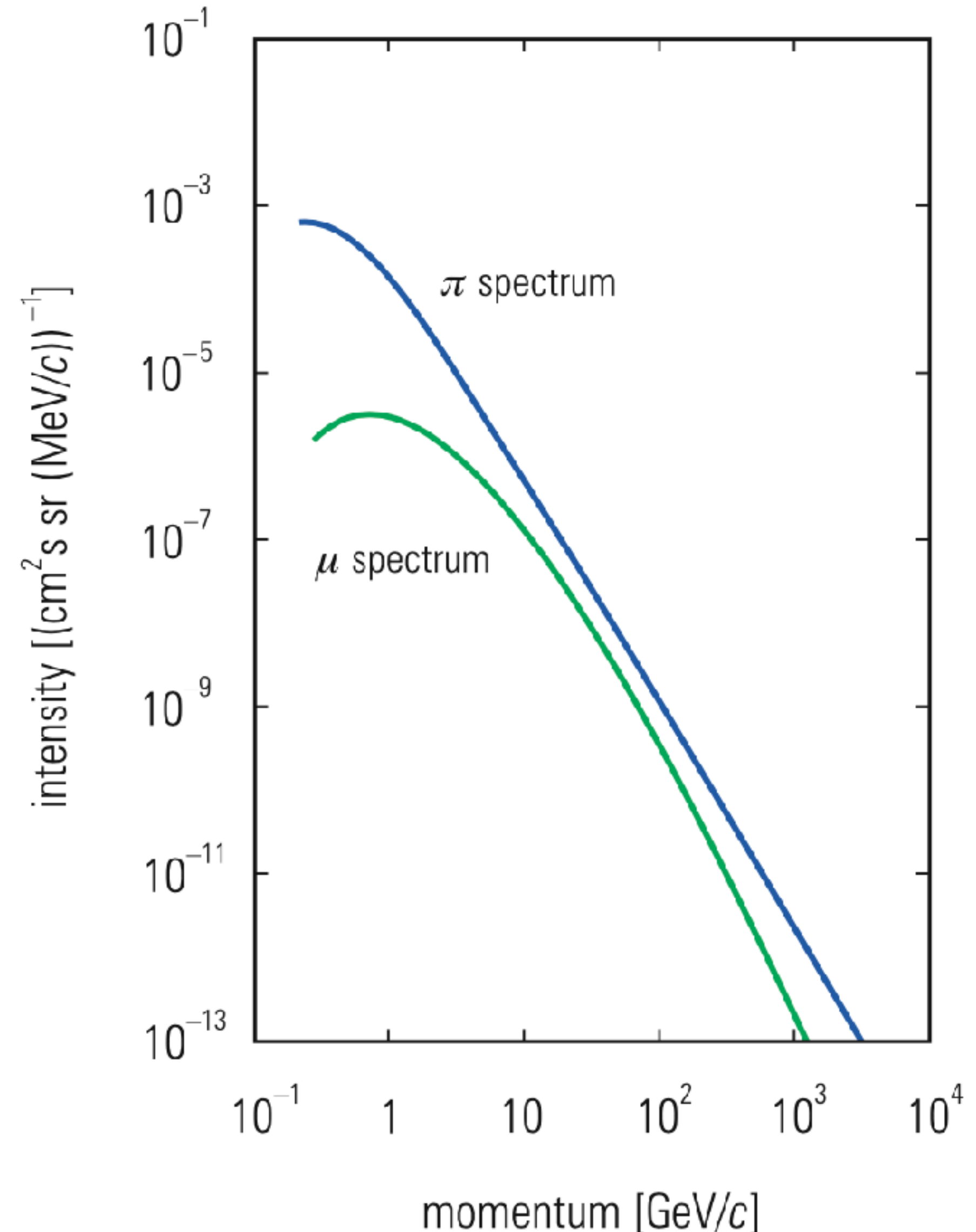
**Fig. 7.13** Muon spectrum at sea level compared to the spectrum of parent pions at production

The **muon spectrum at sea level is therefore a direct consequence of the pion source spectrum**. There are, however, several modifications.

Figure 7.13 shows the parent pion spectrum at the location of production in comparison to the observed sea-level muon spectrum.

**The shape of the muon spectrum agrees relatively well with the pion spectrum for momenta between 10 and 100 GeV/c.**

For energies **below 10 GeV and above 100 GeV the muon intensity**, however, **is reduced** compared to the pion source spectrum.



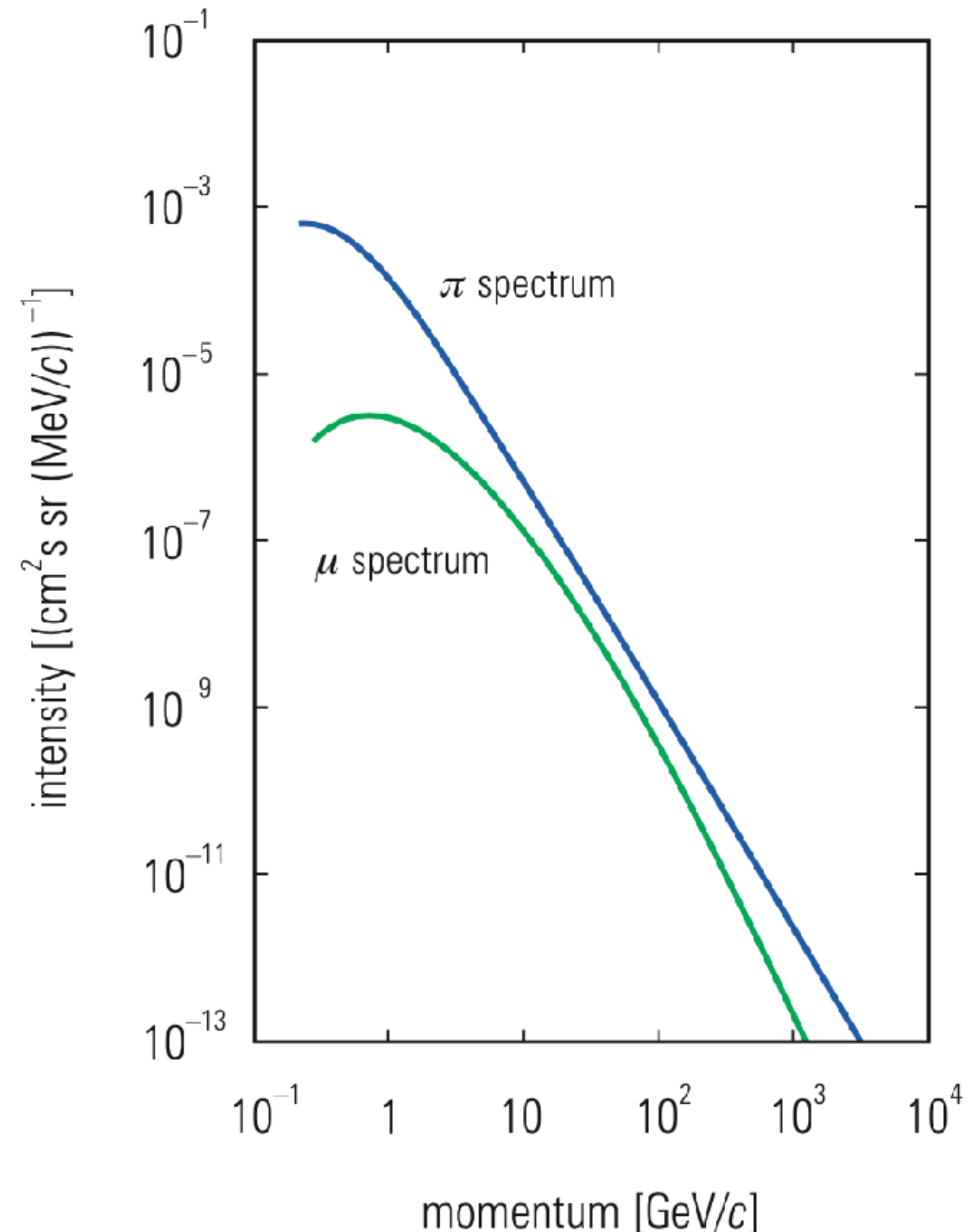
# Cosmic rays at sea level

**Fig. 7.13** Muon spectrum at sea level compared to the spectrum of parent pions at production

For **low energies** the muon decay probability is increased. A muon of 1GeV with a Lorentz factor of  $\gamma = E/m_\mu c^2 = 9.4$  has a mean **decay length** of

$$s_\mu \approx \gamma \tau_\mu c = 6.2 \text{ km} .$$

Since **pions** are typically produced at **altitudes of 15 km and decay relatively fast** (for  $\gamma = 10$  the decay length is only  $s_\pi \approx \gamma \tau_\pi c = 78\text{m}$ ), the **decay muons do not reach sea level** but rather **decay themselves** or get absorbed in the atmosphere.

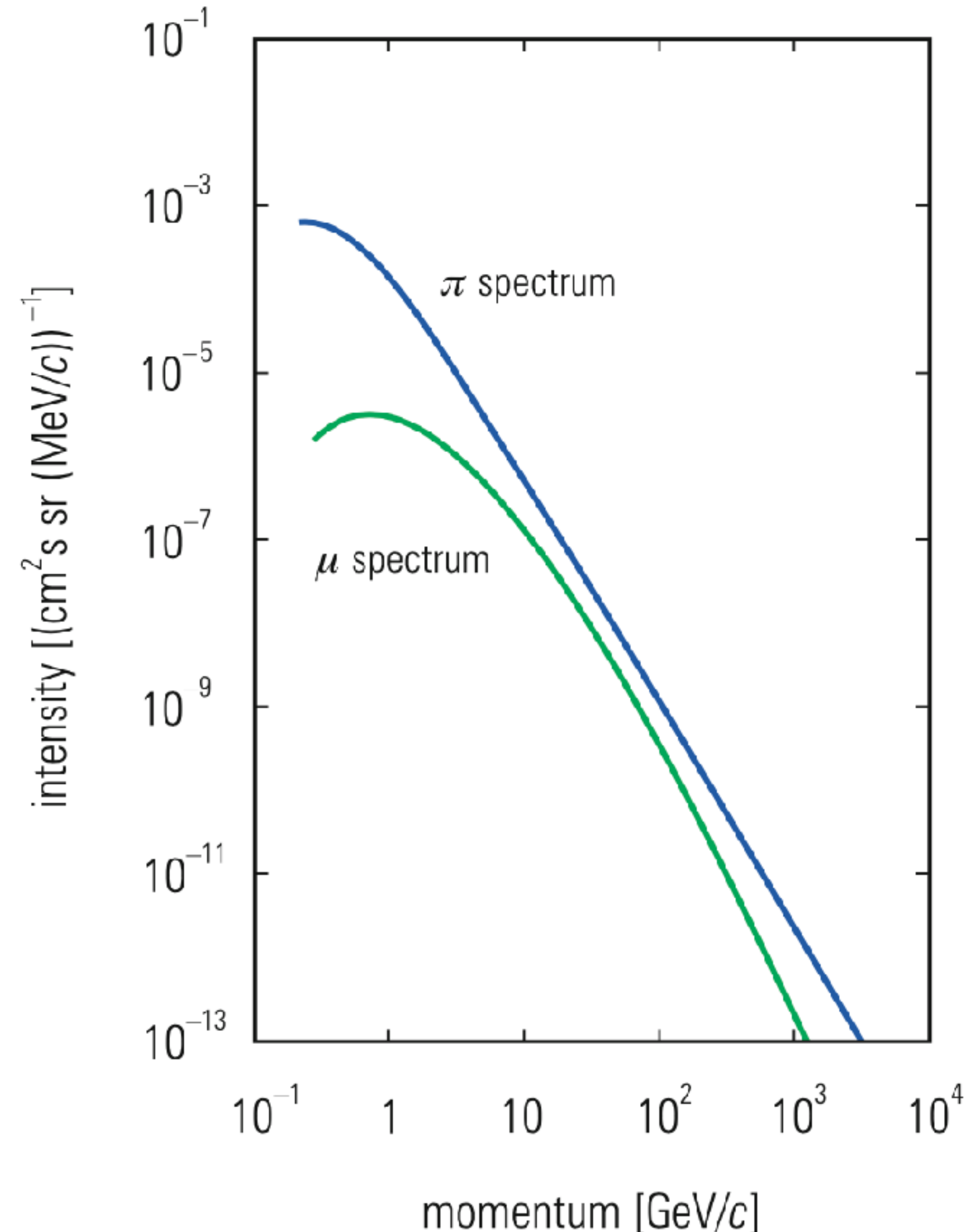


# Cosmic rays at sea level

**Fig. 7.13** Muon spectrum at sea level compared to the spectrum of parent pions at production

At **high energies** the situation is changed. For **pions of 100 GeV** ( $s_\pi = 5.6 \text{ km}$ , corresponding to a column density of  $160 \text{ g/cm}^2$  measured from the production altitude) the interaction probability dominates ( $s_\pi > \lambda$ ). Pions of these energies **will therefore produce further, tertiary pions in subsequent interactions**, which **will also decay** eventually into muons, but **providing muons of lower energy**.

Therefore, the muon spectrum at high energies is always slightly steeper compared to the parent pion spectrum.



# Cosmic rays at sea level

If muons from inclined horizontal directions are considered, a further aspect has to be taken into account. For large zenith angles the parent particles of muons travel **relatively long distances in rare parts of the atmosphere**. Because of the low area density at large altitudes for **inclined directions the decay probability is increased** compared to the interaction probability. Therefore, **for inclined directions pions will produce predominantly high-energy muons in their decay**.

The result of these considerations is in agreement with observation (Fig. 7.14). For about **90 GeV/c the muon intensity at 75° zenith angle starts to outnumber that of the vertical muon spectrum**.

The intensity of muons from horizontal directions at low energies is naturally reduced because of muon decays and absorption effects in the thicker atmosphere at large zenith angles.

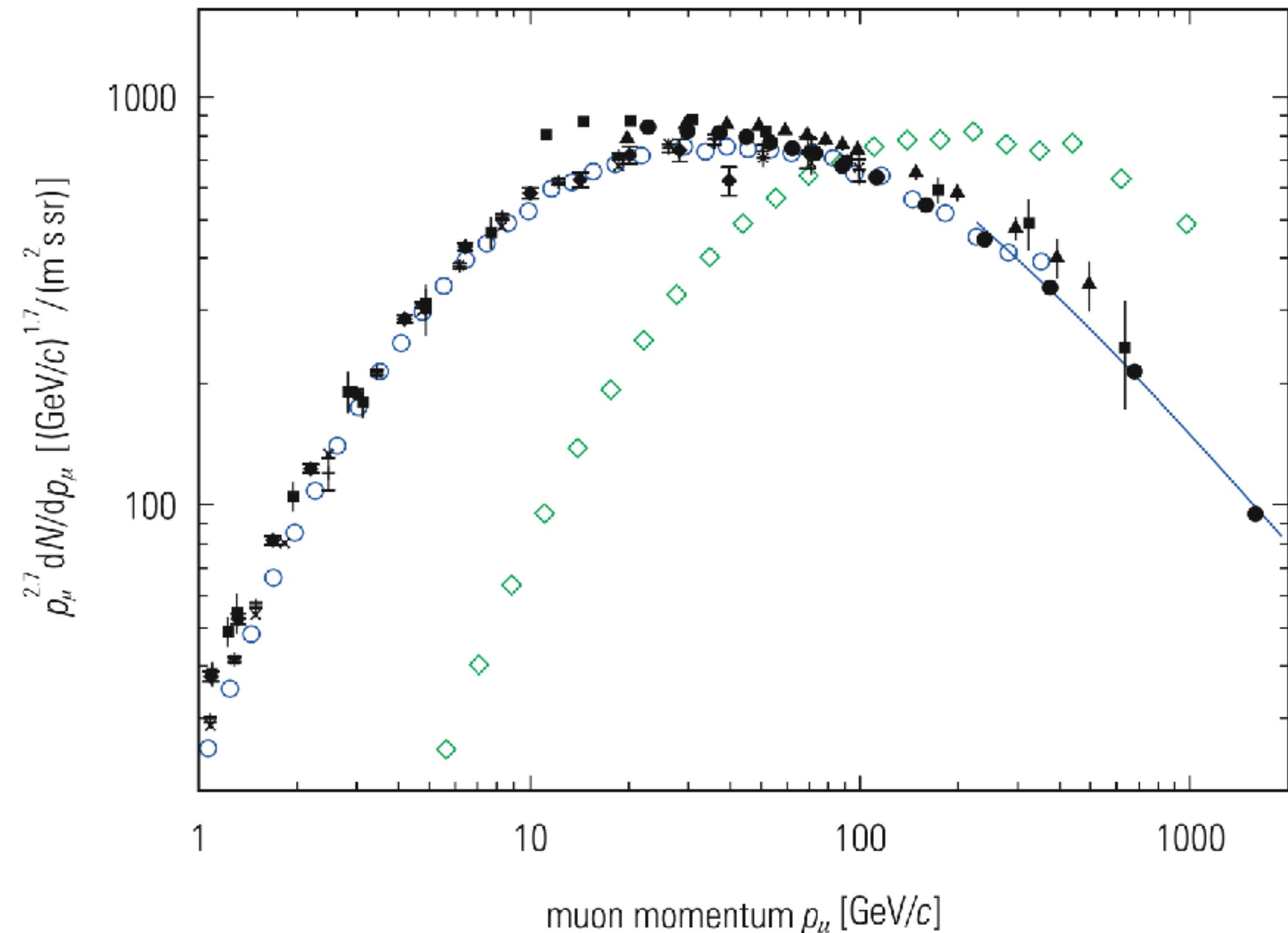


**Fig. 7.14** Sea-level momentum spectrum of muons. The *full circles*, the *open circles*, and *crosses* refer to vertical muons; the *open diamonds* refer to muons from inclined directions ( $75^\circ$ ), and the *solid line at the right-hand side* is the theoretical description of the vertical muon spectrum for energies when the muon decay is negligible (above  $100 \text{ GeV}/(\cos \theta)$ ) and the curvature of the Earth can be neglected ( $\theta$  is the zenith angle) [112]

# Cosmic rays at sea level

The **sea-level muon spectrum** for inclined directions has been measured with **solid-iron momentum spectrometers up to momenta of approximately 20 TeV/c**.

For higher energies the muon intensity decreases steeply. The spectrum of muons beyond 20 TeV/c can be **measured indirectly by observing electromagnetic showers** induced by these muons.

Since the **energy losses** of muons at very high energies are dominated by **bremsstrahlung and direct electron pair production**, which are proportional to the muon energy, these **muon-induced showers allow to infer the muon energy**.

The total intensity of muons, however, is **dominated by low-energy particles**. Because of the zenith angle dependance, the **total muon intensity at sea level varies like**

$$I_\mu(\theta) = I_\mu(\theta = 0) \cos^n \theta$$

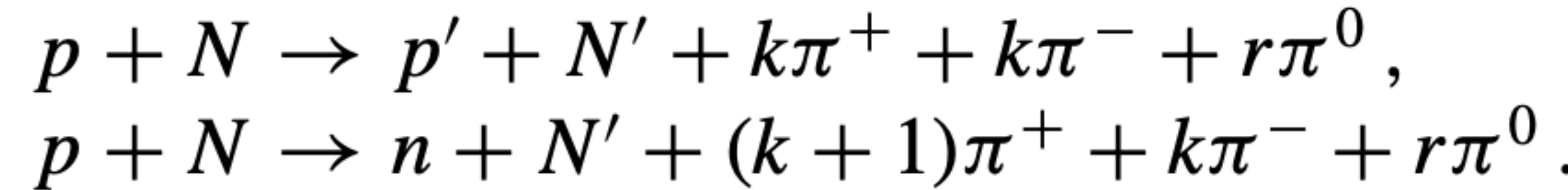
for **not too large zenith angles  $\theta$** .

The exponent of the zenith-angle distribution is obtained to be  **$n = 2$** . This exponent **varies very little**, even at shallow depths underground, **if only muons exceeding a fixed energy are counted**.

# Cosmic rays at sea level

An interesting quantity is the **charge ratio of muons at sea level**.

Since primary cosmic rays are positively charged, this positive charge excess is eventually also transferred to muons. If one assumes that primary protons interact with protons and neutrons of atomic nuclei in the atmosphere, where the multiplicity of produced pions can be quite large, the **charge ratio** of muons,  $N(\mu^+)/N(\mu^-)$ , can be estimated by **considering the possible charge exchange reactions**:



In this equation  **$k$  and  $r$  are the multiplicities** of the produced particle species and  $N$  represents a target nucleon. If one assumes that for the reactions **the cross sections are the same**, **the charge ratio of pions is obtained to be**

$$R = \frac{N(\pi^+)}{N(\pi^-)} = \frac{2k + 1}{2k} = 1 + \frac{1}{2k}$$

# Cosmic rays at sea level

Under these simplifying assumptions one would get for low **energies** and  $k = 2$  a value for the **charge ratio of  $R = 1.25$** .

However, the situation is not as simple as that: **the cross sections are not the same**. The inclusive cross section for the second reaction ( $p + N \rightarrow n + N' + \dots$ ) relative to the first one ( $p + N \rightarrow p' + N' + \dots$ ) is only **30%**, i.e., in **70% of the cases the incident proton stays a proton**, and only in 30% of the cases one gets a leading neutron. This would **lead to a charge ratio smaller than  $R = 1.25$** .

Still, the **theoretically expected charge ratio is higher, close to  $R = 1.25$** , for the following **reason**: the charge ratio is, of course, **linked to the primary spectrum**. The flux of secondary particles (in this case muons) is related to the primary spectrum and to **first approximation it is equal to the primary spectrum multiplied by the so-called spectrum-weighted moment  $Z_{p \rightarrow \mu}$** . This factor is the integral over the inclusive cross section multiplied with the weighting factor  $x^{\gamma-1}$ , where  $x = E_\mu/E_p$  and  $\gamma = 2.7$  for the primary spectrum. The **energy distribution along with the steep spectrum now leads to a charge ratio of about  $R = 1.25$** .

This **charge ratio is eventually transferred to the muons**, which then get a similar ratio.

# Cosmic rays at sea level

Experimentally one observes that the **charge ratio of muons at sea level is constant over a wide momentum range** and takes on a value of

$$N(\mu^+)/N(\mu^-) \approx 1.28$$

Figure 7.15 shows the charge ratio at sea level for muon momenta **up to 2.5 TeV**.

Monte Carlo simulations of the current hadronization models describe the charge ratio well. However, the models SIBYLL and QGSJET show a small deviation from the experimental value of the charge ratio. One has to keep in mind that **most of the models are based on accelerator data**.

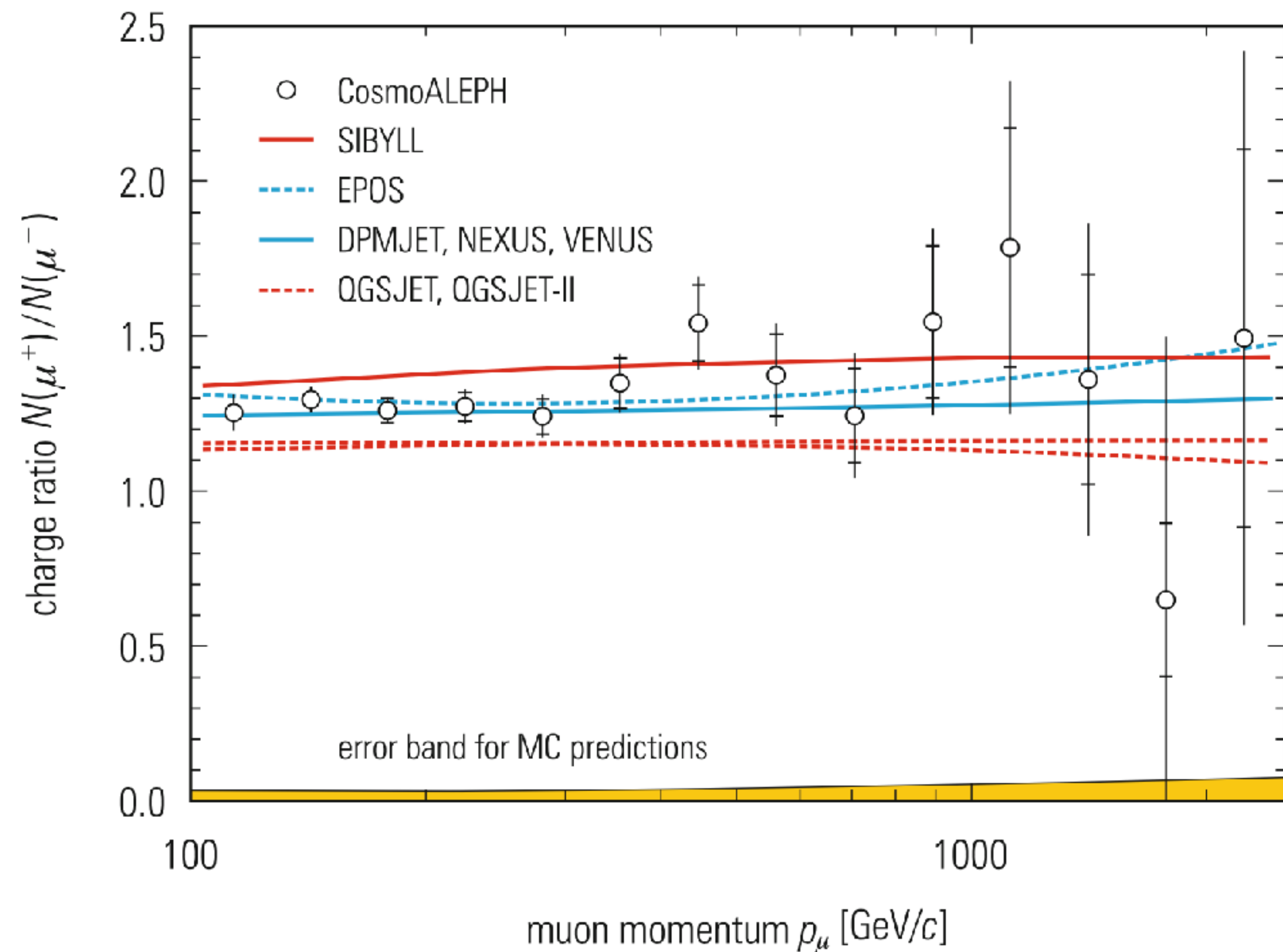


**Fig. 7.15** Charge ratio of muons at sea level. The results from the CosmoALEPH experiment are compared to the predictions of various hadronization models [116]

# Cosmic rays at sea level

$D^0(c\bar{u}), D^+(c\bar{d}), D^-(\bar{c}d)$   
 $B^0(d\bar{b}), B^+(u\bar{b}), B^-(\bar{u}b), B_c^+(c\bar{b}), B_s^0(s\bar{b})$

In addition to ‘classical’ production mechanisms of muons by pion and kaon decays, they **can also be produced in semileptonic decays of charmed mesons**

for example:

$$D^0 \rightarrow K^- + \mu^+ + \nu_\mu$$

$$D^+ \rightarrow \bar{K}^0 + \mu^+ + \nu_\mu$$

$$D^- \rightarrow K^0 + \mu^- + \bar{\nu}_\mu$$

Since these charmed mesons are **very short-lived** ( $\tau_{D^0} \approx 0.4$  ps,  $\tau_{D^\pm} \approx 1.1$  ps), they **decay practically immediately after production** without undergoing interactions themselves → they are a **source of high-energy muons**. Since the production cross section of charmed mesons in proton–nucleon interactions is rather small,  **$D$  decays contribute significantly only at very high energies**. Correspondingly, this is also true for the **semileptonic decays of  $B$  mesons**.

**Draw the Feynman diagram!**

# Cosmic rays at sea level

Figure 7.11 already showed that apart from muons **also some nucleons can be observed at sea level**. These nucleons are **either remnants of primary cosmic rays**, which, however, are reduced in their intensity and energy by multiple interactions, **or they are produced in atmospheric hadron cascades**.

About one **third** of the nucleons at sea level are **neutrons**.

The **proton/muon ratio varies with the momentum** of the particles.

- At **low momenta** ( $\approx 500 \text{ MeV}/c$ ) a  $p/\mu$  ratio  $N(p)/N(\mu)$  of **about 10%** is observed
- **decreasing to larger momenta** at  $1 \text{ GeV}/c$  ( $N(p)/N(\mu) \approx 2\%$ ),
- at  $10 \text{ GeV}/c$   $N(p)/N(\mu) \approx 0.5\%$ ).

The **pion flux is suppressed with respect to the proton flux** by a factor of 20–50, depending on the momentum.

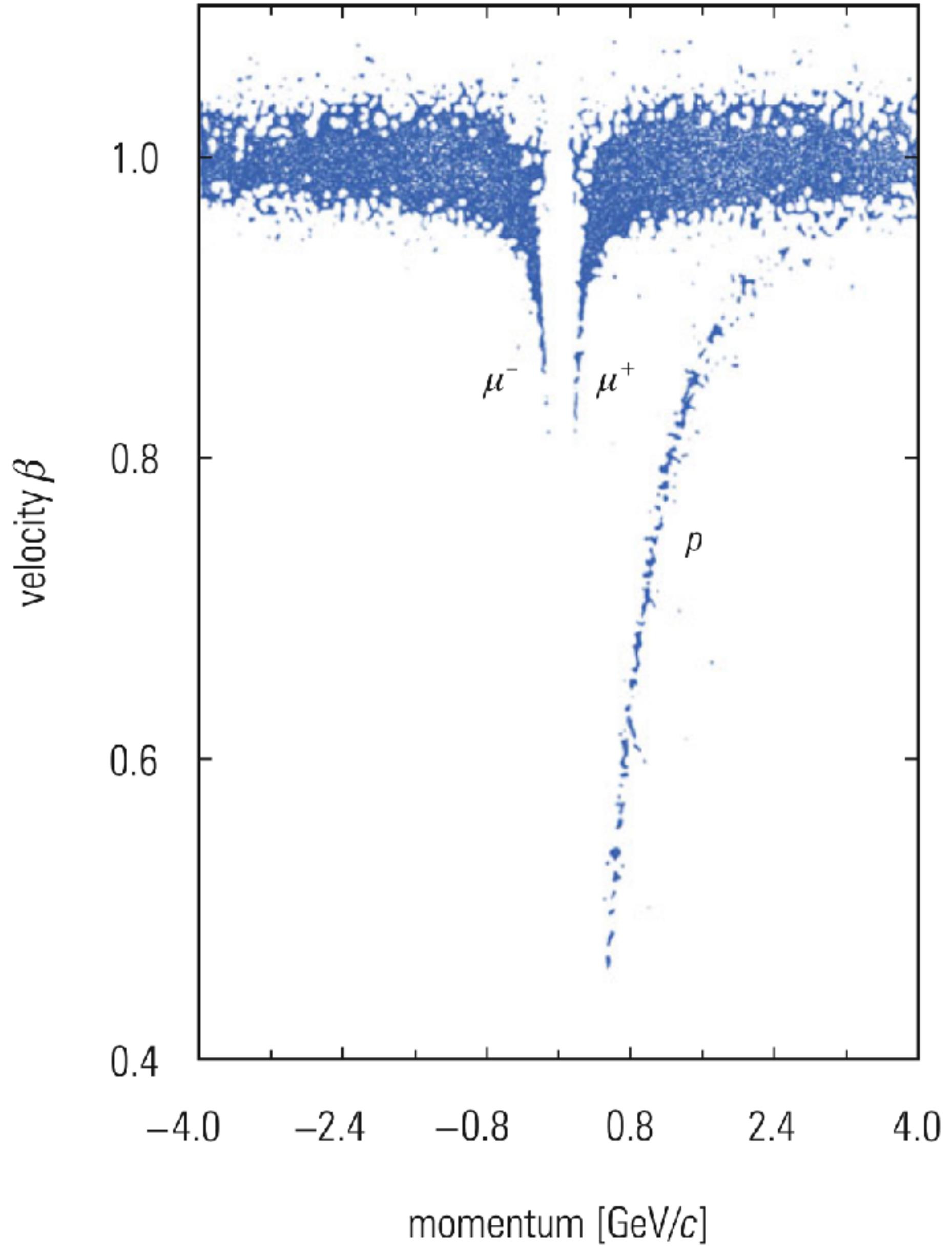


Fig. 7.11 Measurement and identification of charged particles at sea level [113]

# Cosmic rays at sea level

In addition to muons and protons, one **also finds electrons, positrons, and photons at sea level** as a consequence of the **electromagnetic cascades** in the atmosphere.

A certain **fraction of electrons and positrons originates from muon decays**.

Electrons can also be liberated by **secondary interactions of muons ('knock-on electrons'**, see also Fig. 7.16).

The few **pions and kaons observed at sea level** are predominantly produced in **local interactions**.

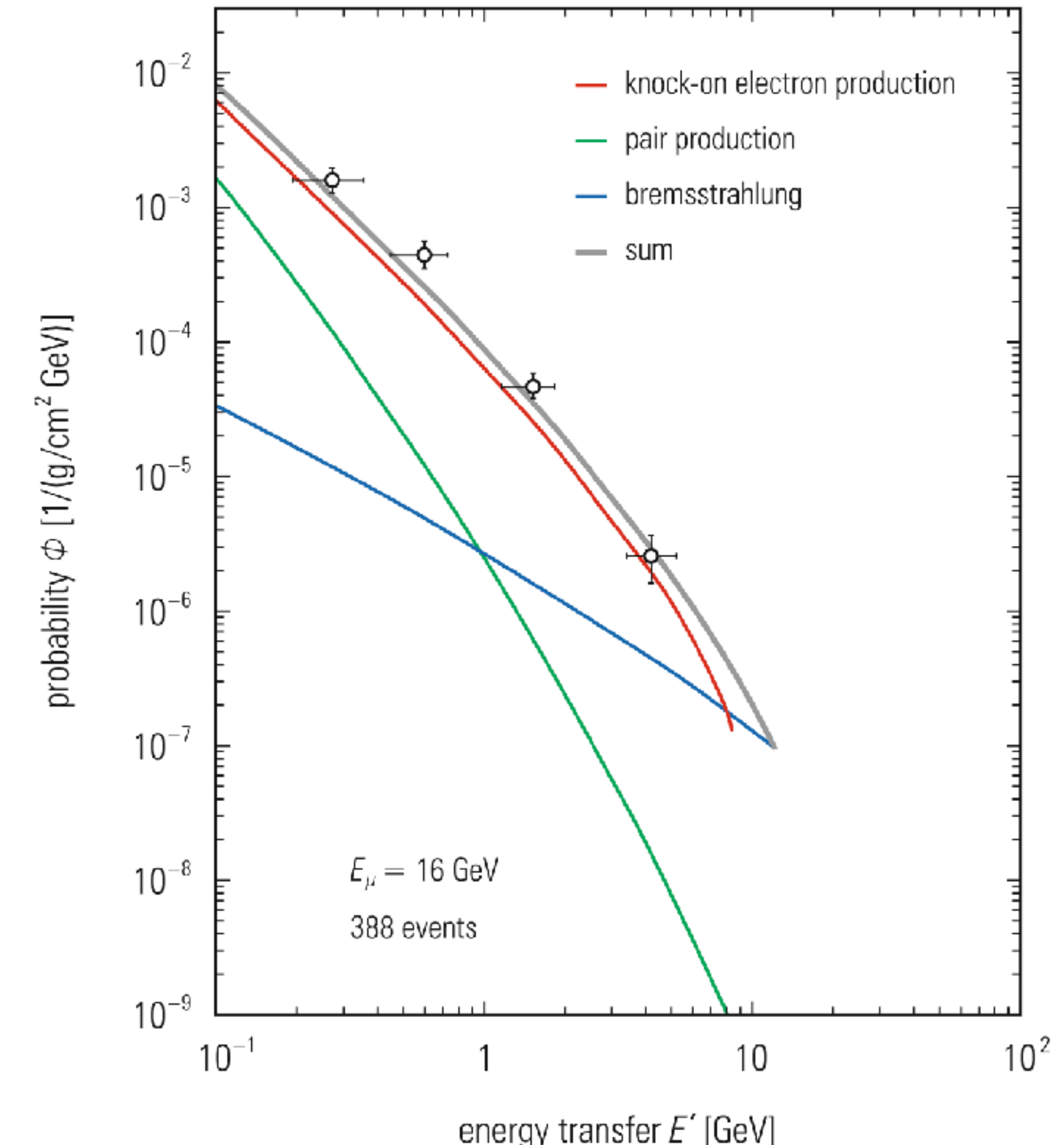


**Fig. 7.16** Experimental results on muon interactions at average muon energies of  $16 \text{ GeV}/c$ . The curves represent predictions of the yield of direct electron pair production (green), bremsstrahlung (blue), knock-on electron production (red), and their sum (grey). At these energies the knock-on production by muons is the dominant process. The vertical scale shows the interaction probability  $\Phi$  per  $\text{g}/\text{cm}^2$ , per  $\text{GeV}$ , and per muon [117]

# Cosmic rays at sea level

Apart from charged particles, **electron and muon neutrinos** are produced in pion, kaon, and muon decays.

The propagation of atmospheric neutrinos has provided new insights for elementary particle physics, such as neutrino oscillations.

Since the parent particles of neutrinos are dominantly pions and kaons and the **decay probability of pions and kaons is increased compared to the interaction probability at inclined directions**, the horizontal neutrino spectra are also harder in comparison to the spectra from vertical directions.

Altogether, **muon neutrinos** would appear to dominate, since the  $(\pi \rightarrow e\nu)$  and  $(K \rightarrow e\nu)$  decays are strongly suppressed due to **helicity conservation**. Therefore, pions and kaons almost exclusively produce muon neutrinos only.

Only in **muon decay equal numbers of electron and muon neutrinos** are produced.

At high energies also **semileptonic decays** of charmed mesons constitute **a source for neutrinos**.

# Cosmic rays at sea level

Based on these ‘classical’ considerations the integral neutrino spectra yield a **neutrino-flavour ratio of**

$$\frac{N(\nu_\mu + \bar{\nu}_\mu)}{N(\nu_e + \bar{\nu}_e)} \approx 2$$

this ratio, however, is **modified by propagation effects like neutrino oscillations.**

# Cosmic rays Underground

Particle composition and energy spectra of secondary cosmic rays **underground** are of **particular importance for neutrino astronomy**.

**Experiments in neutrino astronomy** are usually set up at large depths **underground to provide a sufficient shielding against the other particles from cosmic rays**. Because of the rarity of neutrino events even low fluxes of **residual cosmic rays constitute a background**. In any case it is necessary to know precisely the identity and flux of secondary cosmic rays underground.

Long-range atmospheric muons, secondary particles locally produced by muons, and the interaction products created by atmospheric neutrinos represent the important background sources for neutrino astronomy.

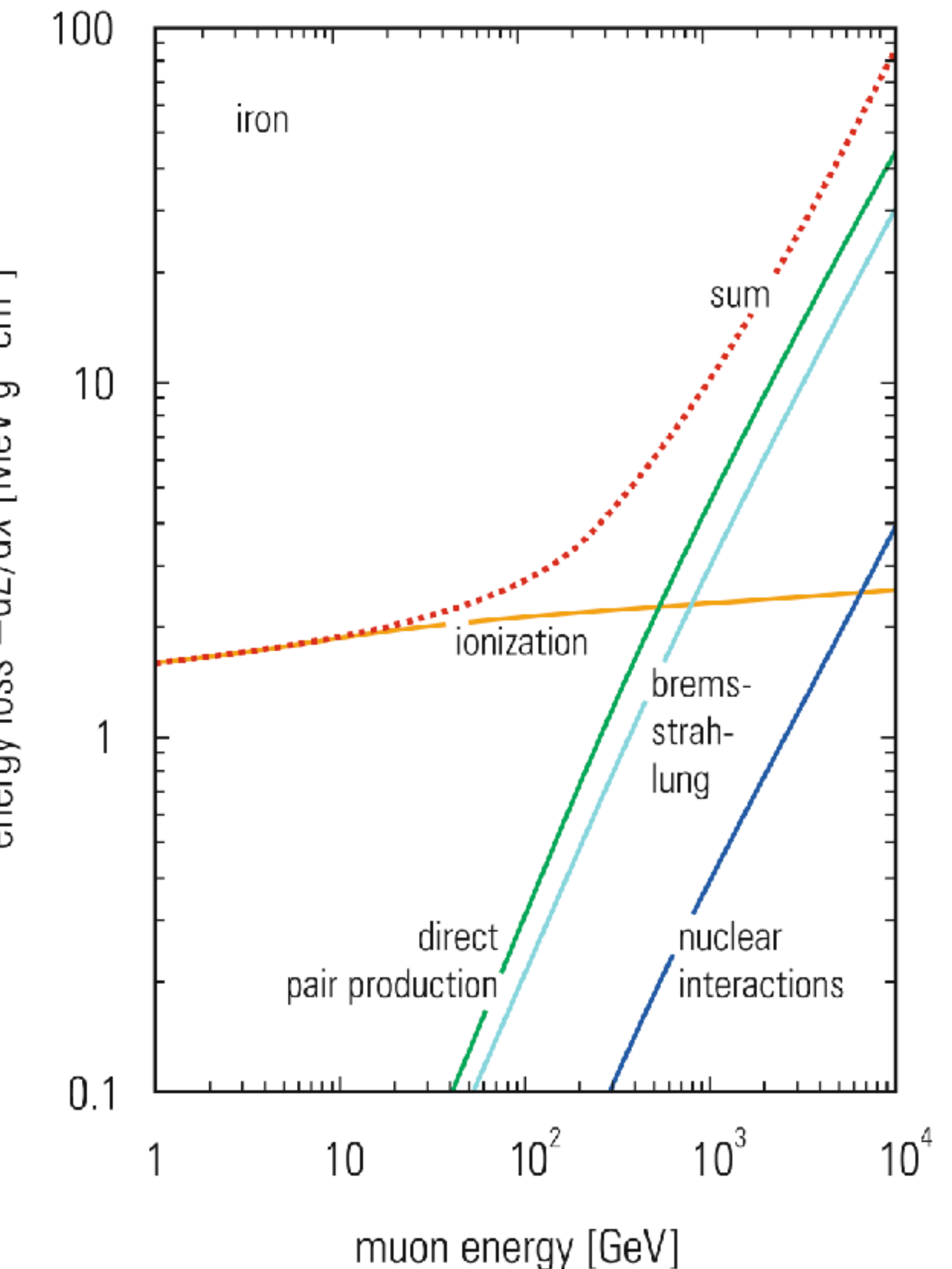
**Muons suffer energy losses by ionization, direct electron–positron pair production, bremsstrahlung, and nuclear interactions.** While the ionization energy loss at high energies is essentially constant, the cross sections for the other **energy-loss processes increase linearly with the energy of the muon**,

$$-\frac{dE}{dx} = a + b E$$

# Cosmic rays Underground

The **energy loss of muons as a function of their energy** is shown in Fig. 7.17 for **iron as absorber material**.

**Fig. 7.17** Contributions to the energy loss of muons in iron



# Cosmic rays Underground

The **energy loss of muons in rock** in its dependence on the muon energy was already shown earlier (Fig. 4.6).

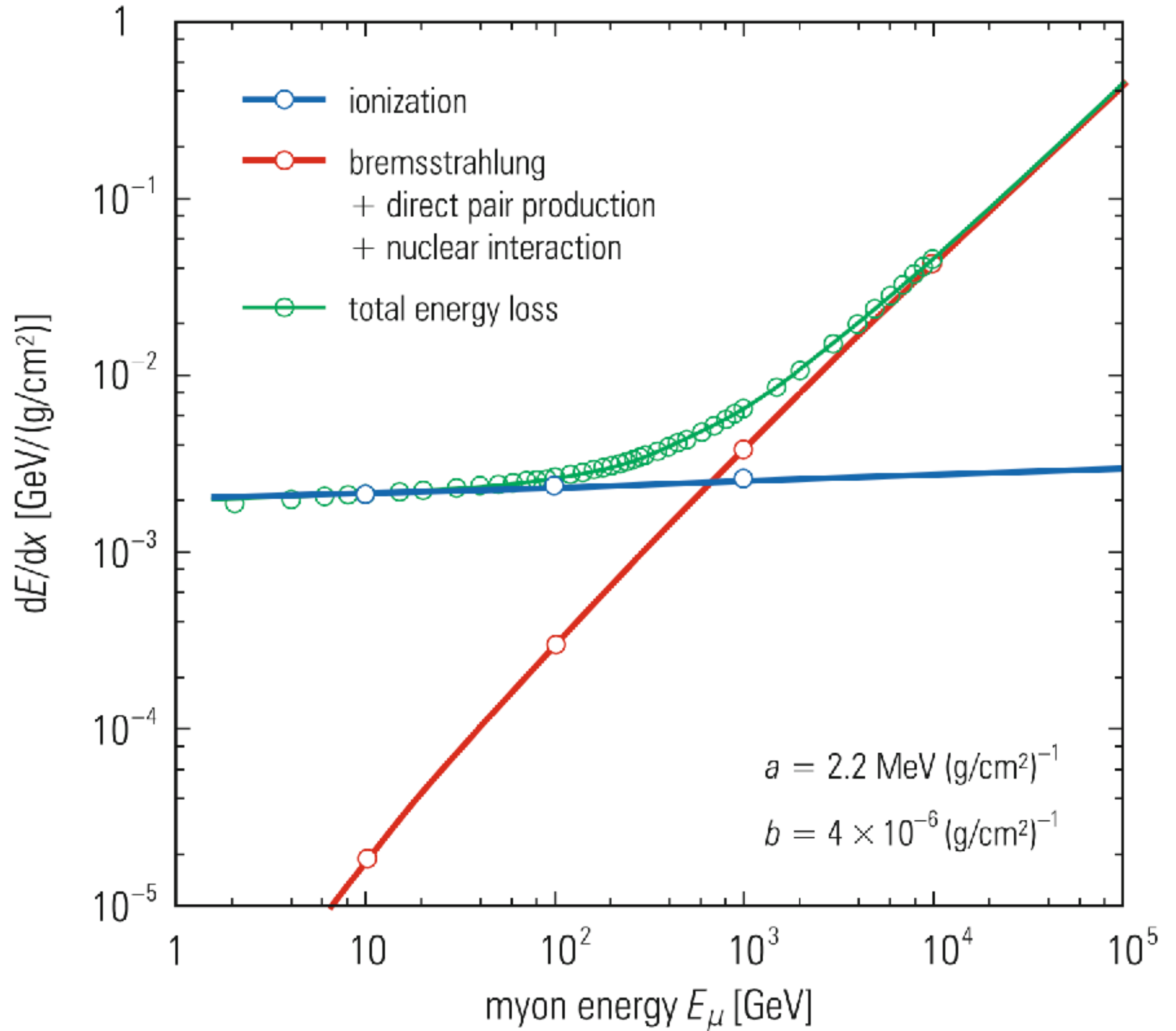


**Fig. 4.6** Energy loss of muons in standard rock [34]

# Cosmic rays Underground

$$-\frac{dE}{dx} = a + b E$$

The energy loss equation allows to work out **the range  $R$  of muons by integration**,

$$R = \int_E^0 \frac{dE}{-dE/dx} = \frac{1}{b} \ln\left(1 + \frac{b}{a} E\right)$$

if it is assumed that the parameters  $a$  and  $b$  are energy independent.

For **not too large energies ( $E < 100\text{GeV}$ ) the ionization energy loss dominates**. In this case  $bE \ll a$  and therefore

$$R = \frac{E}{a}$$

# Cosmic rays Underground

The energy loss of a *minimum-ionizing muon* in the atmosphere is

$$\frac{dE}{dx} = 1.82 \text{ MeV}/(\text{g/cm})^2$$

A muon of **energy 100 GeV** has a range of about 40 000 g/cm<sup>2</sup> in rock corresponding to **160 m (or 400 m water equivalent)**.

An **energy–range relation for standard rock** is shown in Fig. 7.18. Because of the stochastic character of muon interaction processes with large energy transfers (e.g., bremsstrahlung) muons are subject to a **considerable range straggling**.

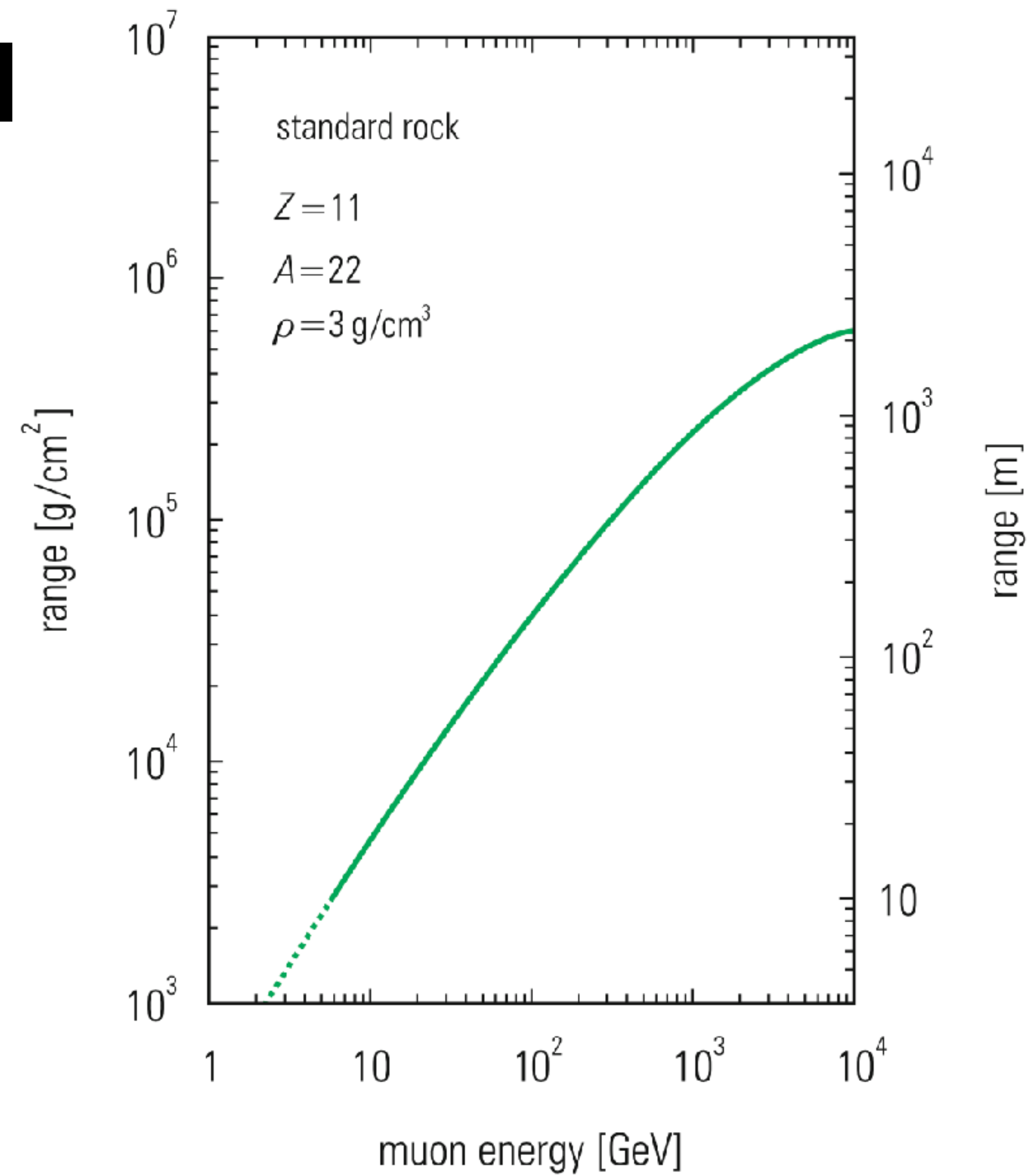


**Fig. 7.18** Range of muons in rock

# Cosmic rays Underground

The knowledge of the **sea-level muon spectrum and the energy-loss processes of muons** allow one to determine the ***depth–intensity relation for muons***.

The **integral sea-level muon spectrum** can be approximated by a **power law**

$$N(>E) = A E^{-\gamma}$$

Using the energy–range relation, the depth–intensity relation is obtained,

$$N(>E, R) = A \left[ \frac{a}{b} (e^{bR} - 1) \right]$$

For high energies ( $E_\mu > 1$  TeV,  $bE \gg a$ ) the exponential dominates and one obtains

$$N(>E, R) = A \left( \frac{a}{b} \right)^{-\gamma} e^{-\gamma bR}$$

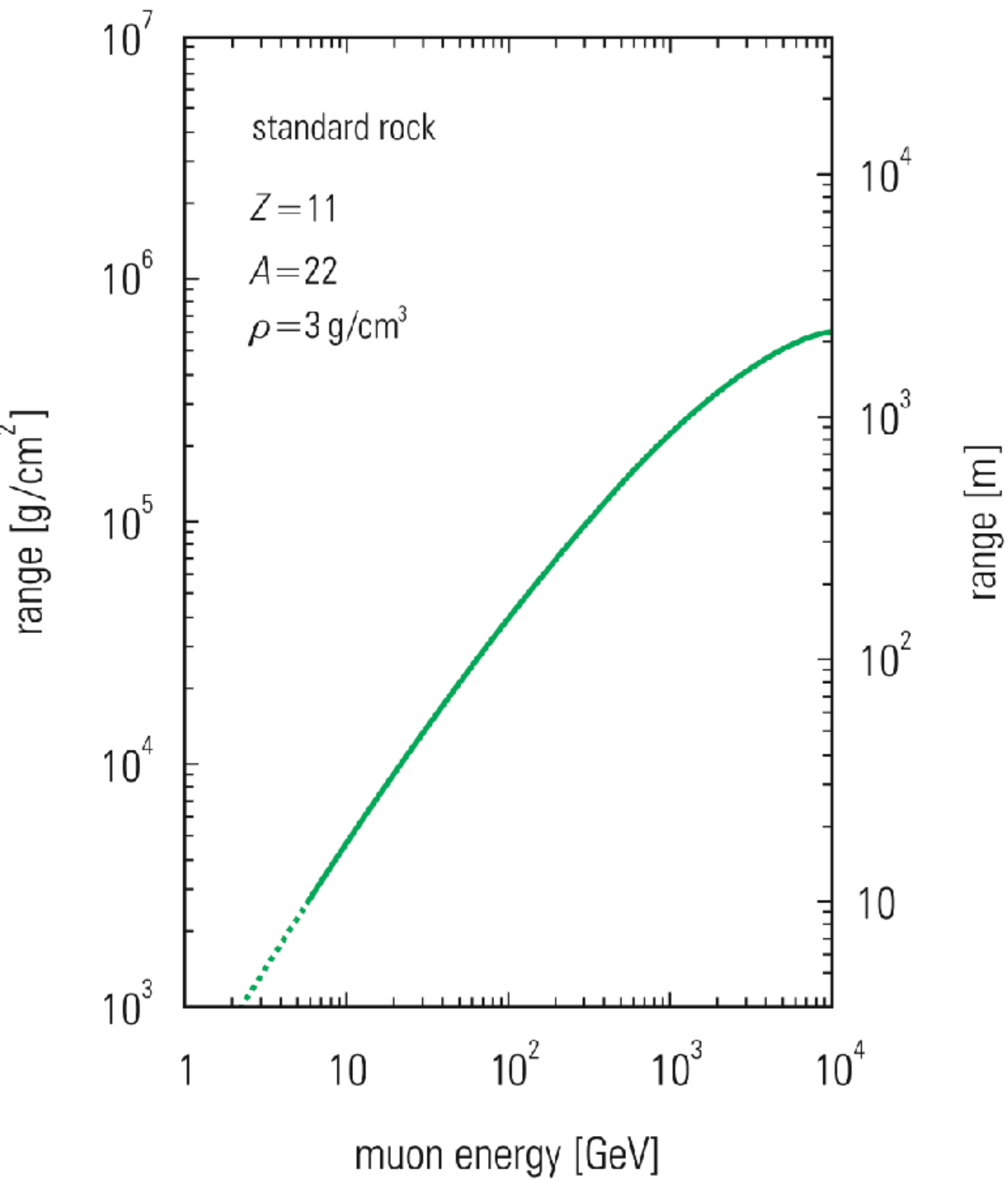


**Fig. 7.18** Range of muons in rock

# Cosmic rays Underground

For inclined directions the absorbing ground layer increases like  $1/\cos \theta = \sec \theta$  ( $\theta$ —zenith angle) for a flat overburden, so that for muons from inclined directions one obtains a depth–intensity relation of

$$N(>E, R, \theta) = A \left(\frac{a}{b}\right)^{-\gamma} e^{-\gamma b R \sec \theta}$$

For shallower depths, the equations lead to a power law

$$N(>E, R) = A (aR)^{-\gamma}$$

# Cosmic rays Underground

The measured depth–intensity relation for vertical directions is plotted in Fig. 7.19.

From depths of 10km water equivalent ( $\approx 4000\text{m}$  rock) onwards muons induced by atmospheric neutrinos dominate the muon rate.

Because of the low interaction probability of neutrinos the neutrino-induced muon rate does not depend on the depth.

At large depths (>10 km w.e.) a neutrino telescope with a collection area of  $100 \times 100 \text{ m}^2$  and a solid angle of  $\pi$  would still measure a background rate of 10 events per day.

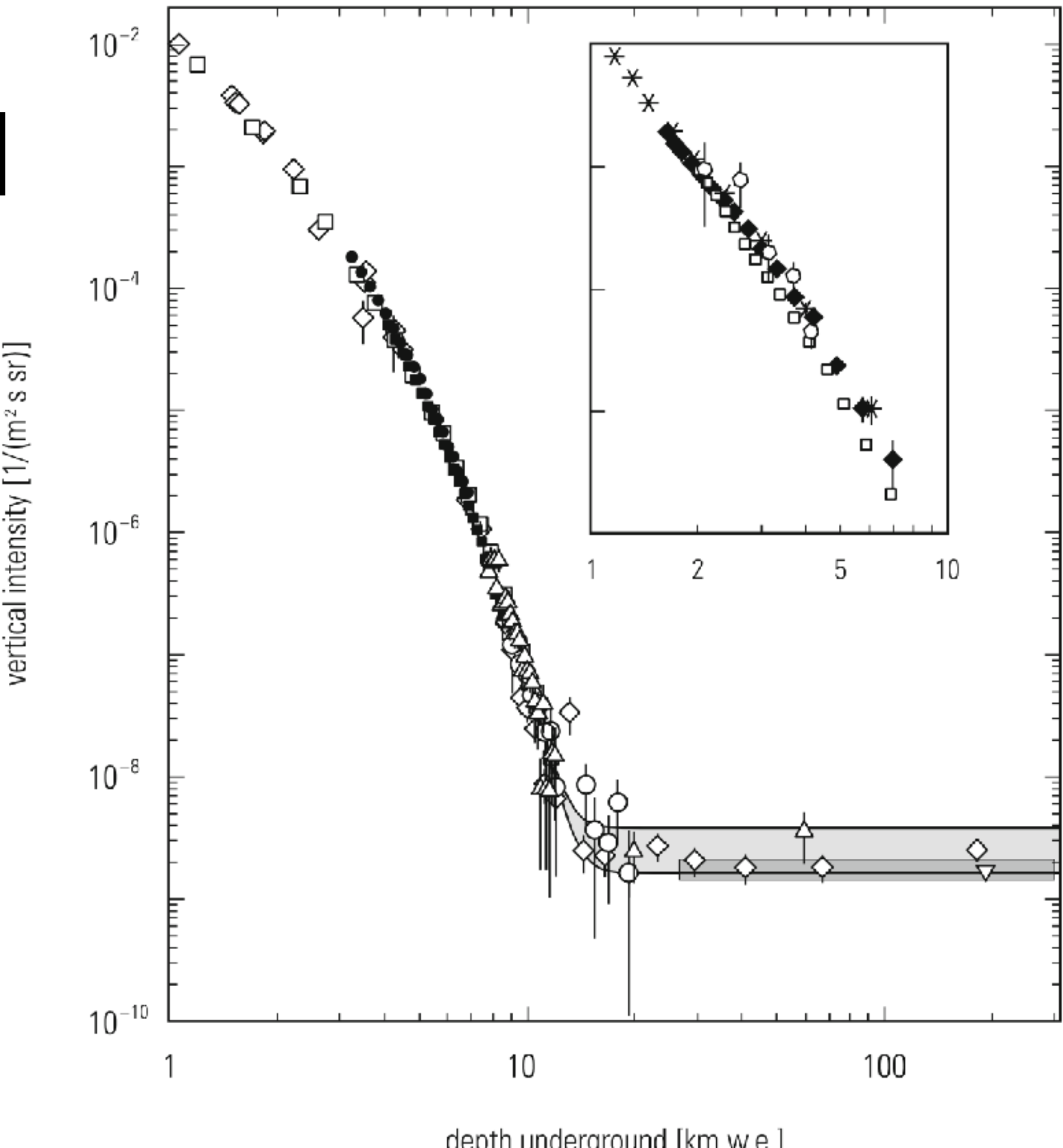


**Fig. 7.19** Depth–intensity relation for muons from vertical directions. The *grey band* at large depths represents the flux of  $\nu$ -induced muons with energies above 2 GeV. The *upper line* refers to horizontal  $\nu$ -induced muons, the *lower one* for vertical upward  $\nu$ -induced muons. The *stronger shadowed area* at very large depths shows the measurements of the Super-Kamiokande experiment. The *inset* shows the vertical depth–intensity relation for water and ice. The *left-hand vertical scale in the inset* can be read from the *corresponding vertical scale in the main diagram*. The *horizontal scale* is in km w.e. [118]

# Cosmic rays Underground

The **zenith-angle distributions of atmospheric muons for depths of 1500 and 7000 meter water equivalent** are shown in Fig. 7.20.

For large zenith angles the flux decreases steeply, because the thickness of the overburden increases like  $1/\cos\theta$ . Therefore, **at large depths and from inclined directions neutrino-induced muons dominate**.

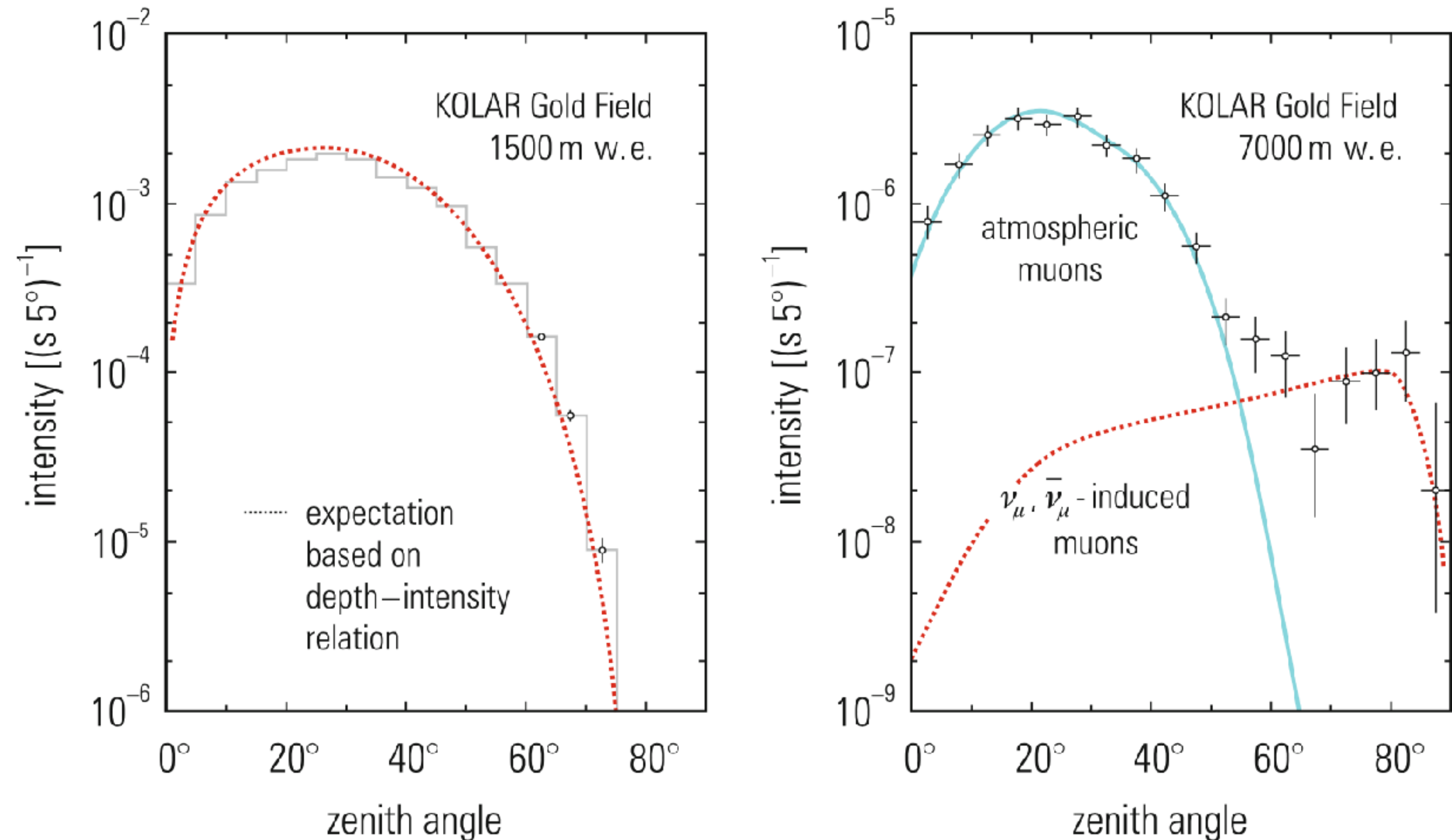


**Fig. 7.20** Zenith-angle distribution of atmospheric muons at depths of 1500 and 7000m w.e. [119]

# Cosmic rays Underground

For not too large zenith angles and depths the **zenith-angle dependence of the integral muon spectrum** can still be represented by

$$I(\theta) = I(\theta = 0) \cos^n \theta$$

(Fig. 7.21). For large depths the exponent  $n$  in this distribution, however, gets very large, so that it is

$$N(>E, R, \theta) = A \left( \frac{a}{b} \right)^{-\gamma} e^{-\gamma b R \sec \theta}$$

preferable to use instead.

The **average energy of muons at sea level is in the range of several GeV**. Absorption processes in rock reduce predominantly the intensity at low energies.

Therefore, the **average muon energy of the muon spectrum increases with increasing depth**.

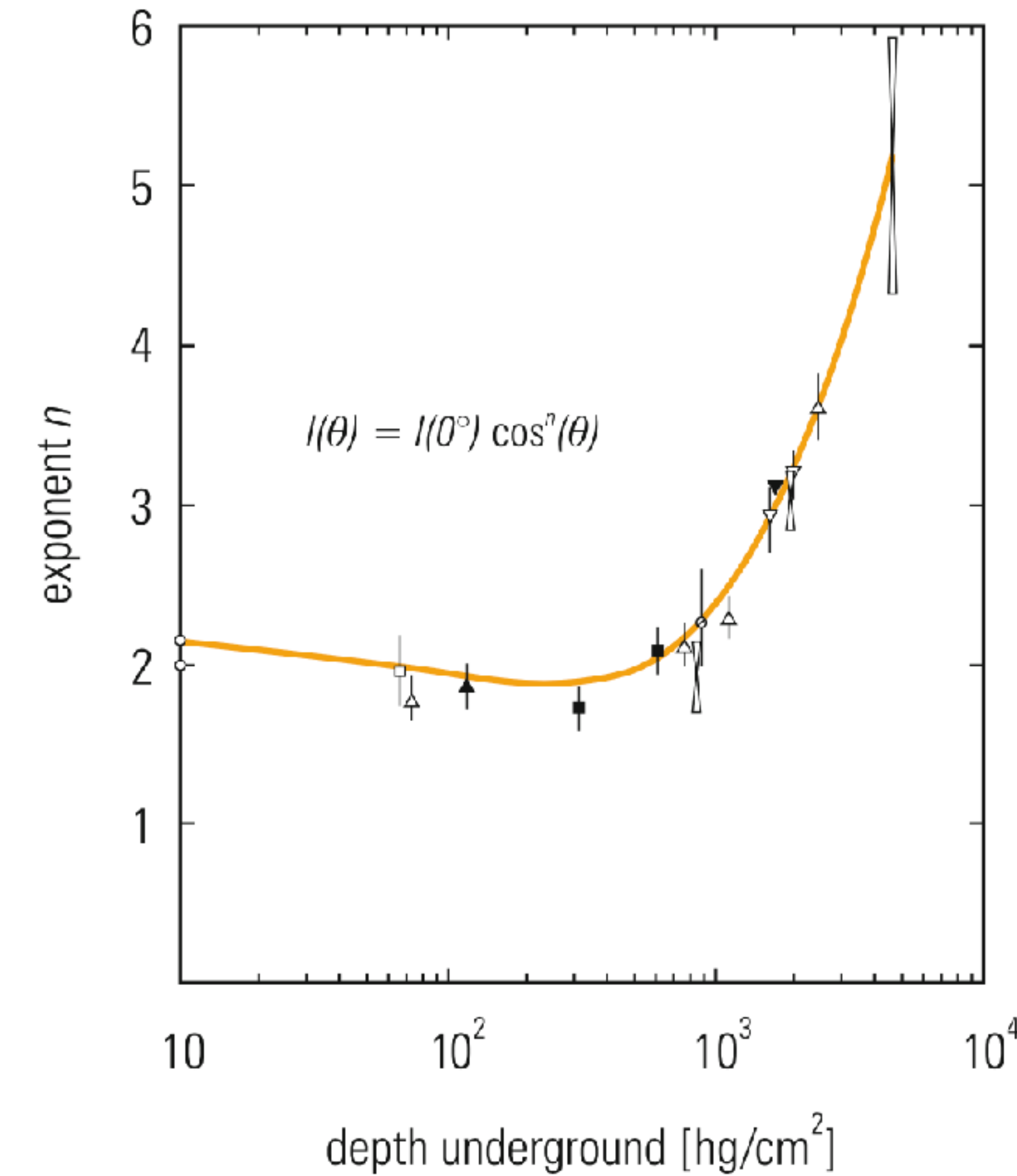


Fig. 7.21 Variation of the exponent  $n$  of the zenith-angle distribution of muons with depth [120]

# Cosmic rays Underground

Muons of high energy can also **produce other secondary particles** in local interactions. Since **low-energy muons can be identified by their ( $\mu \rightarrow e \nu \nu$ ) decay** with the characteristic decay time in the microsecond range, the measurement of **stopping muons underground provides an information about local production processes**.

A certain **fraction of stopping muons is produced locally by low-energy pions**, which decay relatively fast into muons. The flux of penetrating muons decreases rapidly with increasing depth, therefore **the ratio of stopping to penetrating muons is strongly influenced by stopping muons induced by neutrino interactions** for depths larger than 5000 m w.e.

The knowledge of the particle composition at large depths below ground represents an important information for neutrino astrophysics.

Also **remnants of extensive air showers, which developed in the atmosphere, are measured underground**. Electrons, positrons, photons, and hadrons are completely absorbed already in relatively shallow layers of rock. Therefore, **only muons and neutrinos** of extensive air showers penetrate to larger depths.

# Cosmic rays Underground

The primary interaction vertex of particles that initiate the air showers is typically at an atmospheric altitude of 15 km.

Since secondary particles in hadronic cascades have transverse momenta of typically 300 MeV/c or less, the high-energy muons essentially follow the shower axis. For primaries of energy around  $10^{14}$  eV lateral displacements of energetic muons ( $\approx 1$  TeV) at shallow depths underground of less than a meter exclusively caused by transferred transverse momenta are obtained. Typical multiple-scattering angles for energetic muons ( $\approx 100$  GeV) in thick layers of rock (50–100 m) are on the order of a few mrad.

The multiplicity of produced secondary particles increases with energy of the initiating particle (for a 1-TeV proton the charged multiplicity of particles for proton–proton interactions is about 15). Since the secondaries produced in these interactions decay predominantly into muons, one observes bundles of nearly parallel muons underground in the cores of extensive air showers.

# Cosmic rays Underground

Figure 7.22 shows such a **shower with more than 50 parallel muons observed** by the ALEPH experiment at a **depth of 320 m w.e.**

Apart from the numerous muons also a **knock-on electron is visible in the central tracking chamber**. The electron is knocked out of an atom by one of the muons, and—because of its **low energy**—is forced by the **strong transverse magnetic field on a circular track** in the time projection chamber. In contrast, the **tracks of the energetic muons are hardly bent** in the magnetic field of 1.5 tesla strength.

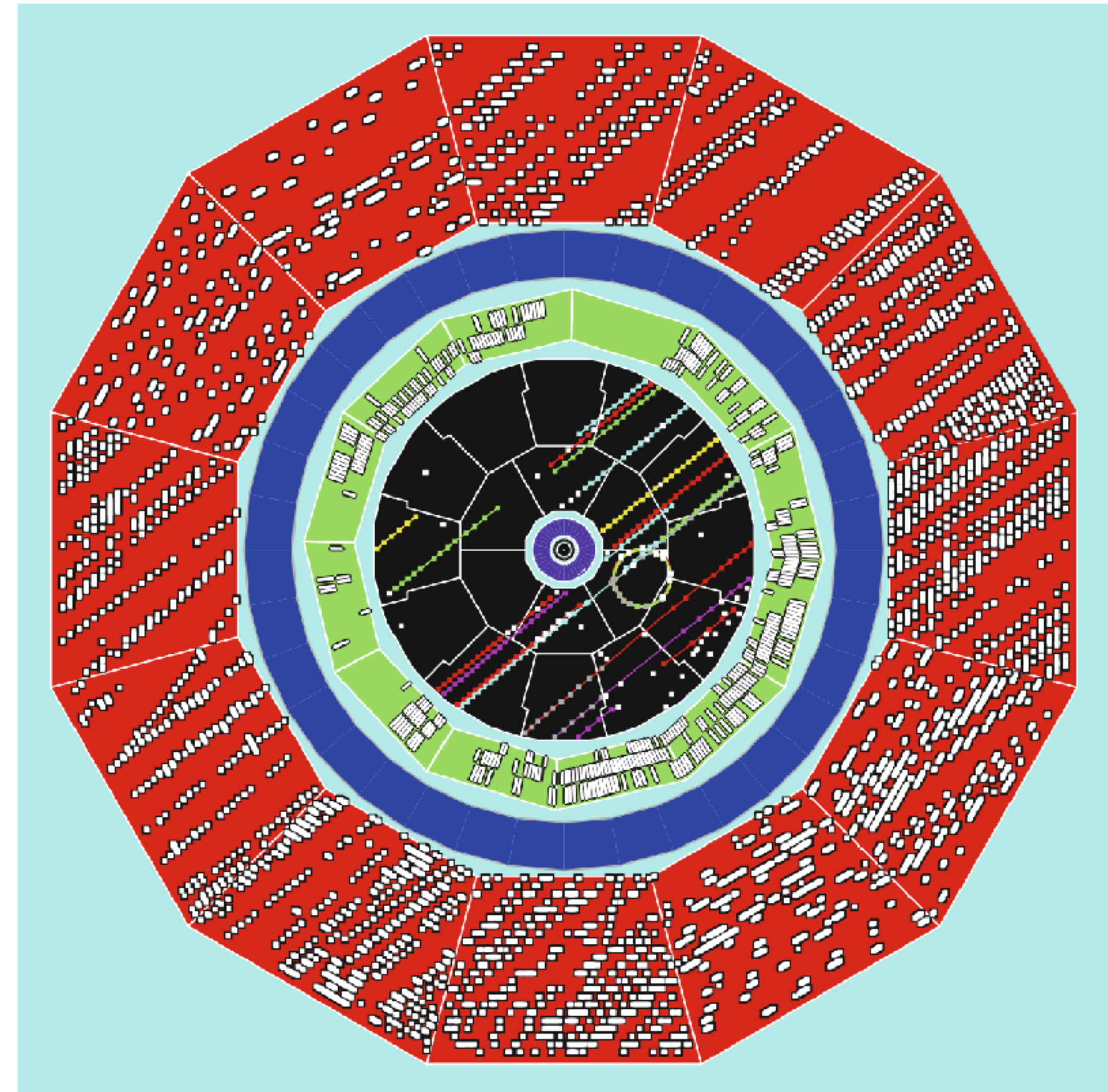


Fig. 7.22 Muon shower in the CosmoALEPH experiment (detector diameter about 10m) [121]

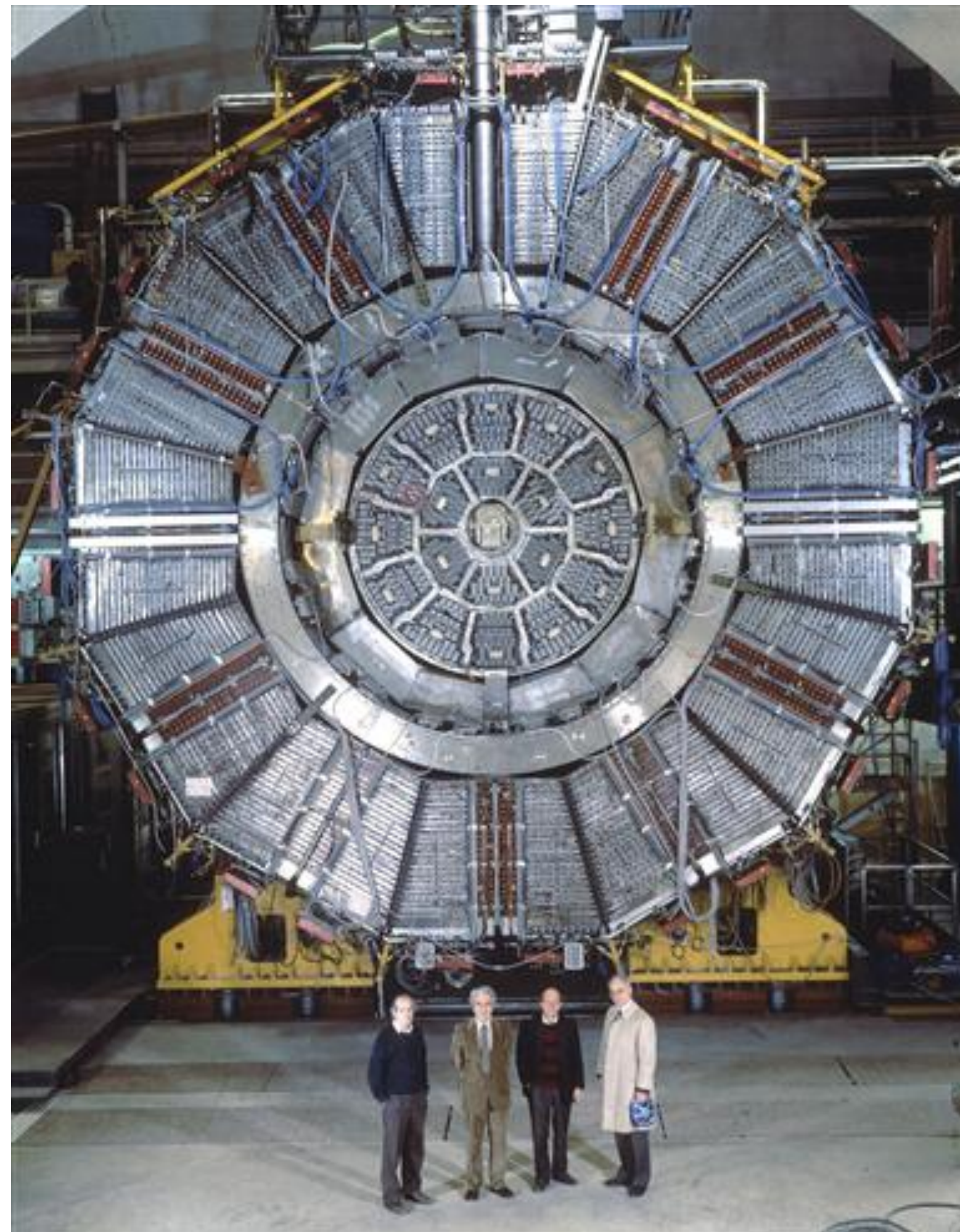
# ALEPH

**ALEPH was a particle detector on the Large Electron-Positron collider (LEP).** It was designed to explore the physics predicted by the Standard Model and to search for physics beyond it.

ALEPH first measured events in LEP in July 1989. LEP operated at around 91 GeV – the predicted optimum energy for the formation of the Z particle. From 1995 the accelerator operated at energies up to 200 GeV, above the threshold for producing pairs of W particles.

The ALEPH detector was built in cylindrical layers around a beam pipe made of beryllium, with the electron-positron collision point in the middle. The whole system was housed inside a 12-sided cylinder and surrounded by a muon-detection system.

The ATLAS and CMS detectors which appeared later on the Large Hadron Collider follow a similar "onion-layer" configuration to ALEPH.



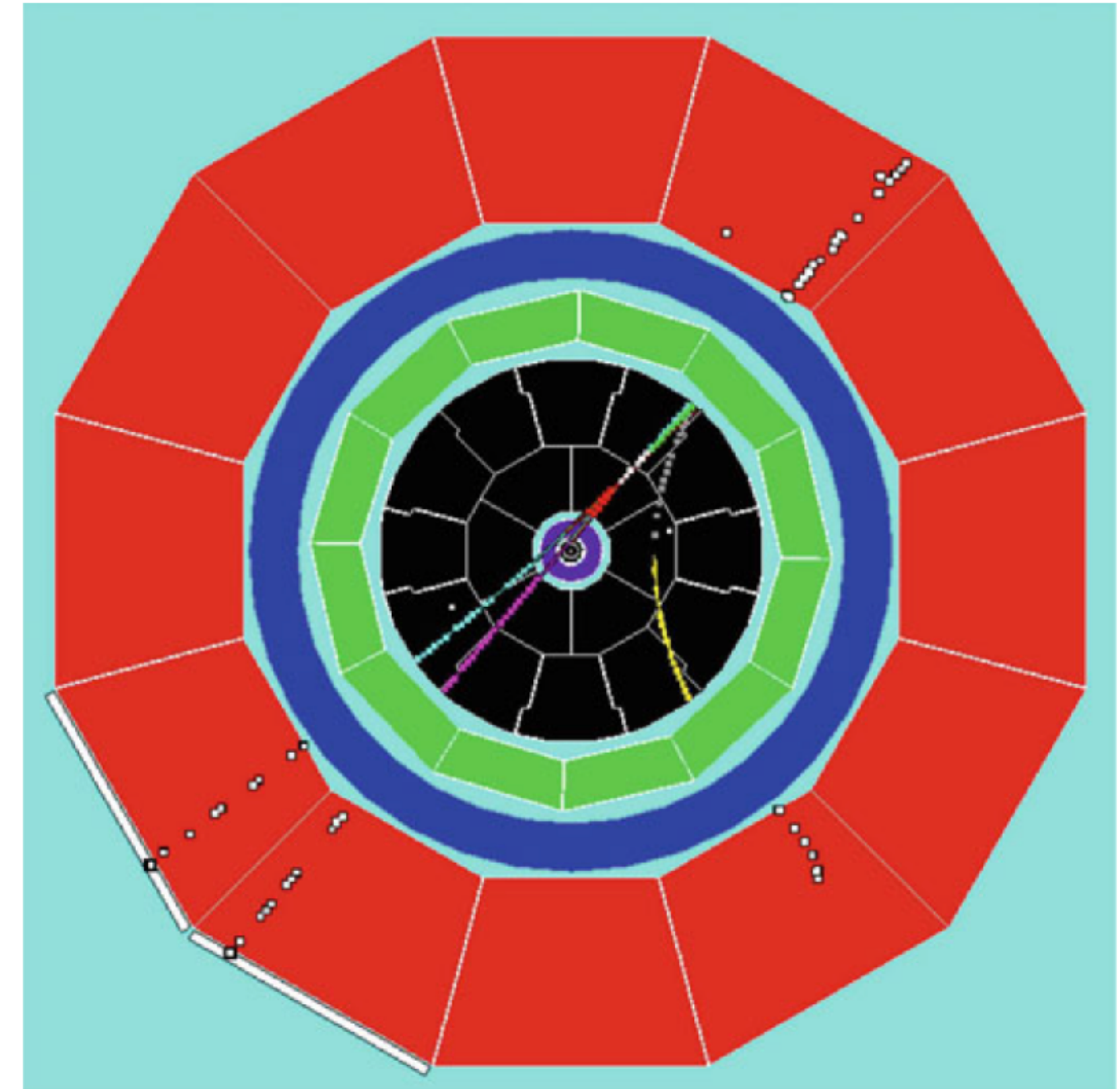
# Cosmic rays Underground

Figure 7.23 shows a relatively **rare example of a muon pair production by a cosmic-ray muon** in the CosmoALEPH experiment:

a so-called **muon-trident process**

$$\mu + N \rightarrow \mu + \mu^+ + \mu^- + N .$$

The cross section of this process is quite small.



**Fig. 7.23** Muon pair production by a cosmic-ray muon in the CosmoALEPH experiment [122]

# Cosmic rays Underground

**High-energy muons are produced by high-energy primaries** and, in particular, **muon showers correlate with even higher primary energies**. Therefore, one is tempted to **localize extraterrestrial sources** of high-energy cosmic rays via the arrival directions of single or multiple muons.

Since **Cygnus X3** has been claimed to **emit photons with energies up to  $10^{16}$  eV**, this astrophysical source also represents an excellent candidate for the acceleration of high-energy charged primary cosmic rays.

Cygnus X3 at a distance of approximately 33 000 light-years is an **X-ray binary** consisting of **a pulsar and a stellar companion**. The material flowing from the companion into the direction of the pulsar forms an **accretion disk around the pulsar**. If apparently photons of very high energy can be produced, one would expect them to **originate from the  $\pi^0$  decay ( $\pi^0 \rightarrow \gamma \gamma$ )**.

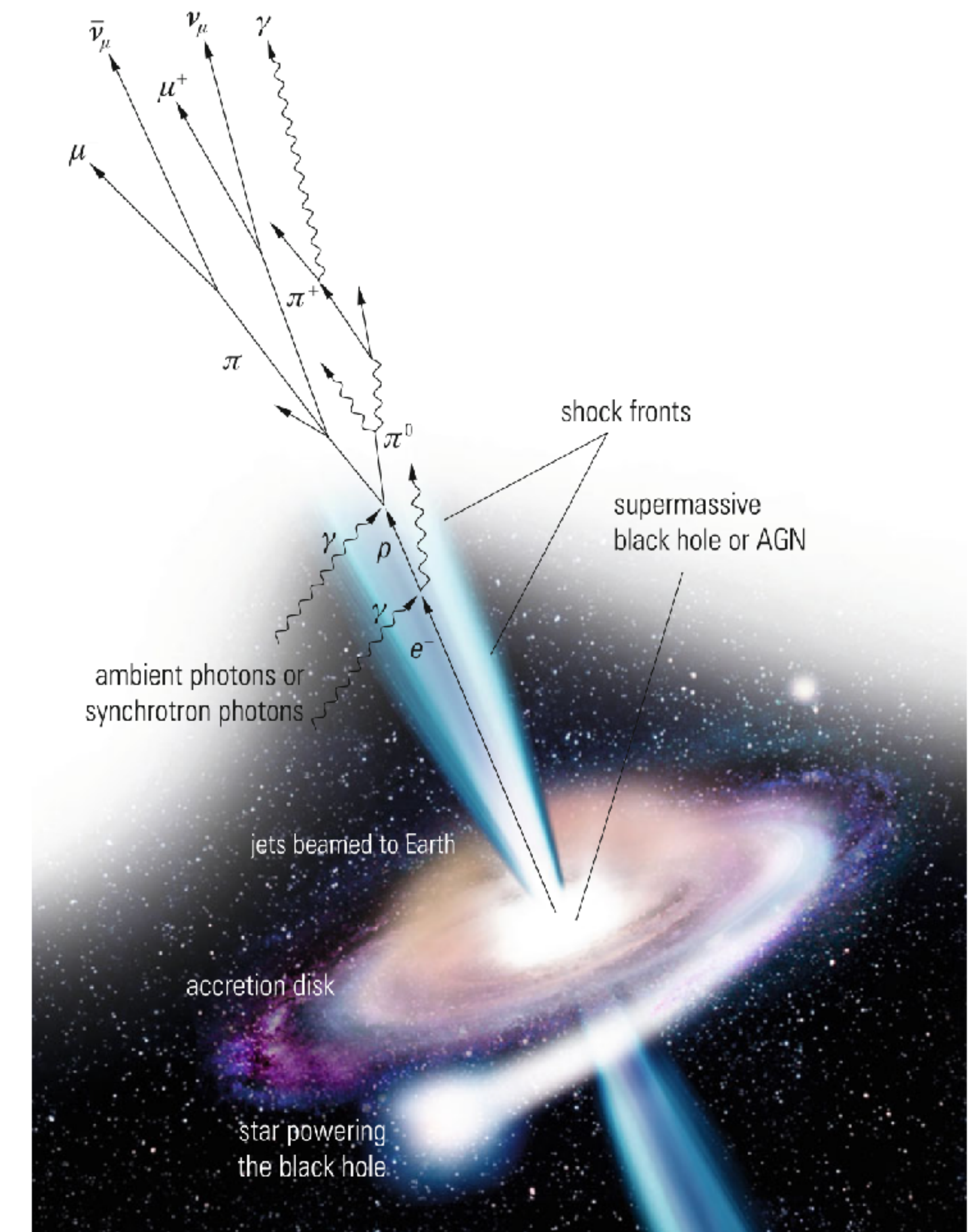


**Fig. 5.9** Acceleration model for relativistic jets powered by a black hole or an active galactic nucleus. The various reactions are only sketched

# Cosmic rays Underground

**Neutral pions** are usually produced **in proton interactions**. Therefore, the source should also be able to **produce charged pions** and via **their decay muons and muon neutrinos**.

Because of their short lifetime, muons would never survive the 33 000-light-year distance from Cygnus X3 to Earth, so that **a possible muon signal must be caused by neutrino-induced muons**.

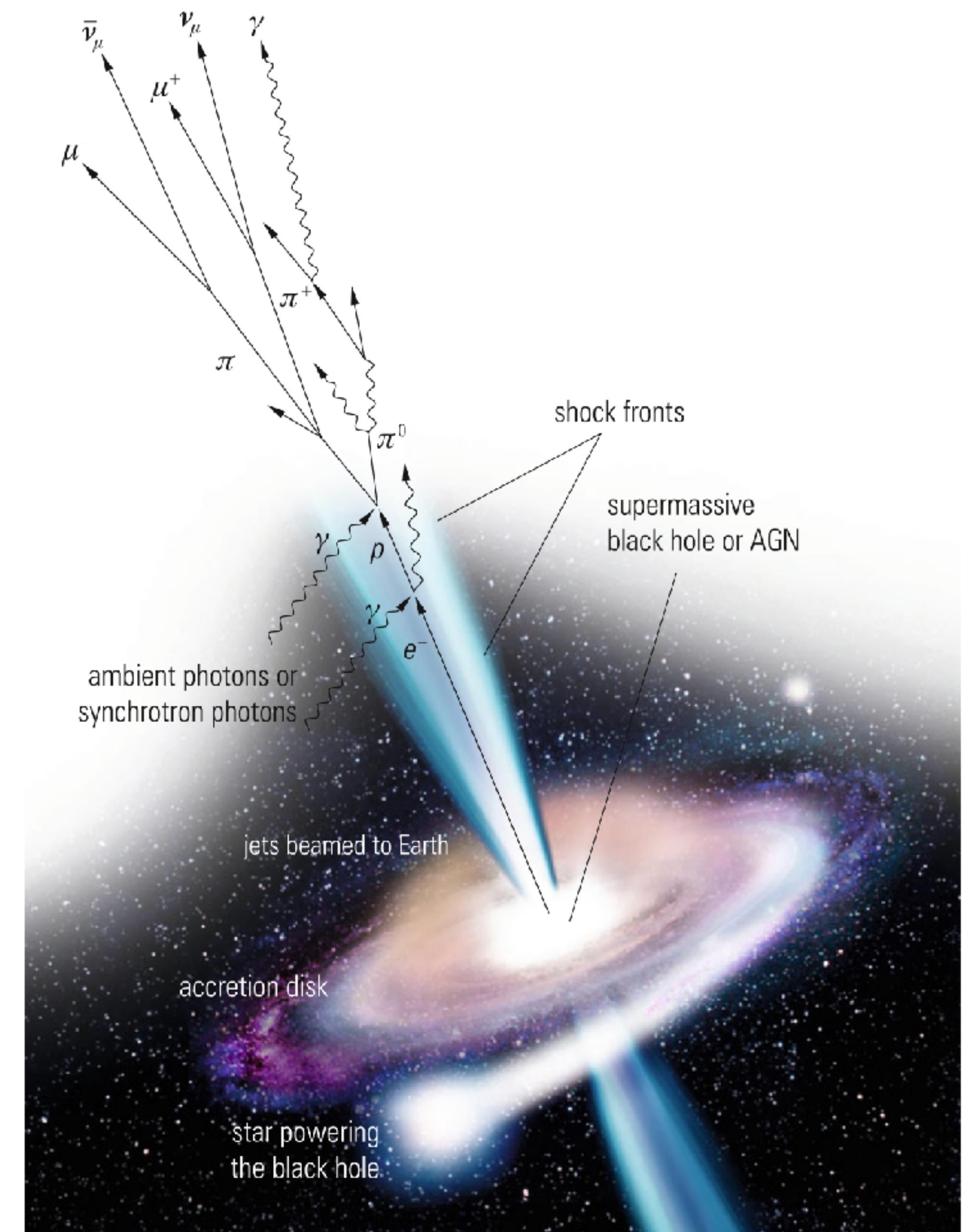


**Fig. 5.9** Acceleration model for relativistic jets powered by a black hole or an active galactic nucleus. The various reactions are only sketched

# Cosmic rays Underground

Unfortunately, muons and multi-muons observed in the Frejus experiment also from the directions of Cygnus X3 are predominantly of atmospheric origin and **do not confirm that Cygnus X3 is a strong source of high-energy particles**. The primary particles themselves accelerated in the source could in principle point back to the source when measured on Earth. However, the arrival direction of primary charged particles from Cygnus X3 could also have been completely randomized by the irregular galactic magnetic field. Muon production by neutrinos from Cygnus X3 would have been a rare event, which would have required an extremely massive detector to obtain a significant rate.

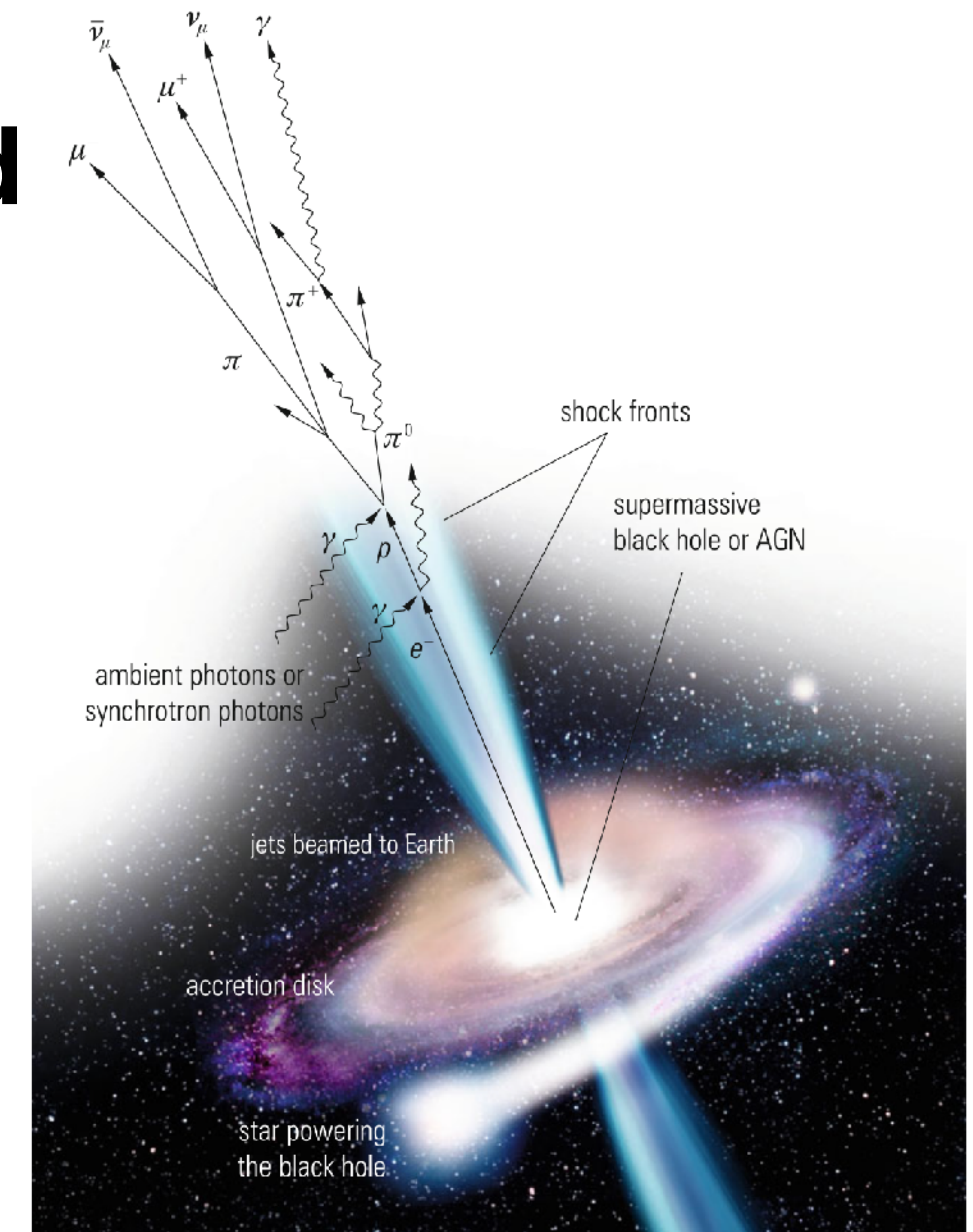


**Fig. 5.9** Acceleration model for relativistic jets powered by a black hole or an active galactic nucleus. The various reactions are only sketched

# Cosmic rays Underground

Figure 7.24, on the other hand, presents an ***anti source*** of cosmic rays, namely, a **shadow of the Moon** in the light of TeV muons as measured in the ICECUBE experiment.

**The Moon absorbs a certain amount of primary cosmic rays.** Therefore, one expects a **reduction of cosmic particles from this direction** and thereby also a **deficit of muons**, which would have otherwise been created in the atmosphere. The width of the Moon shadow was in agreement with simulations.

This also demonstrates that the ICECUBE experiment is able to search for cosmic point sources. The measurement of the Moon shadow also allows to infer an angular resolution of ICECUBE.

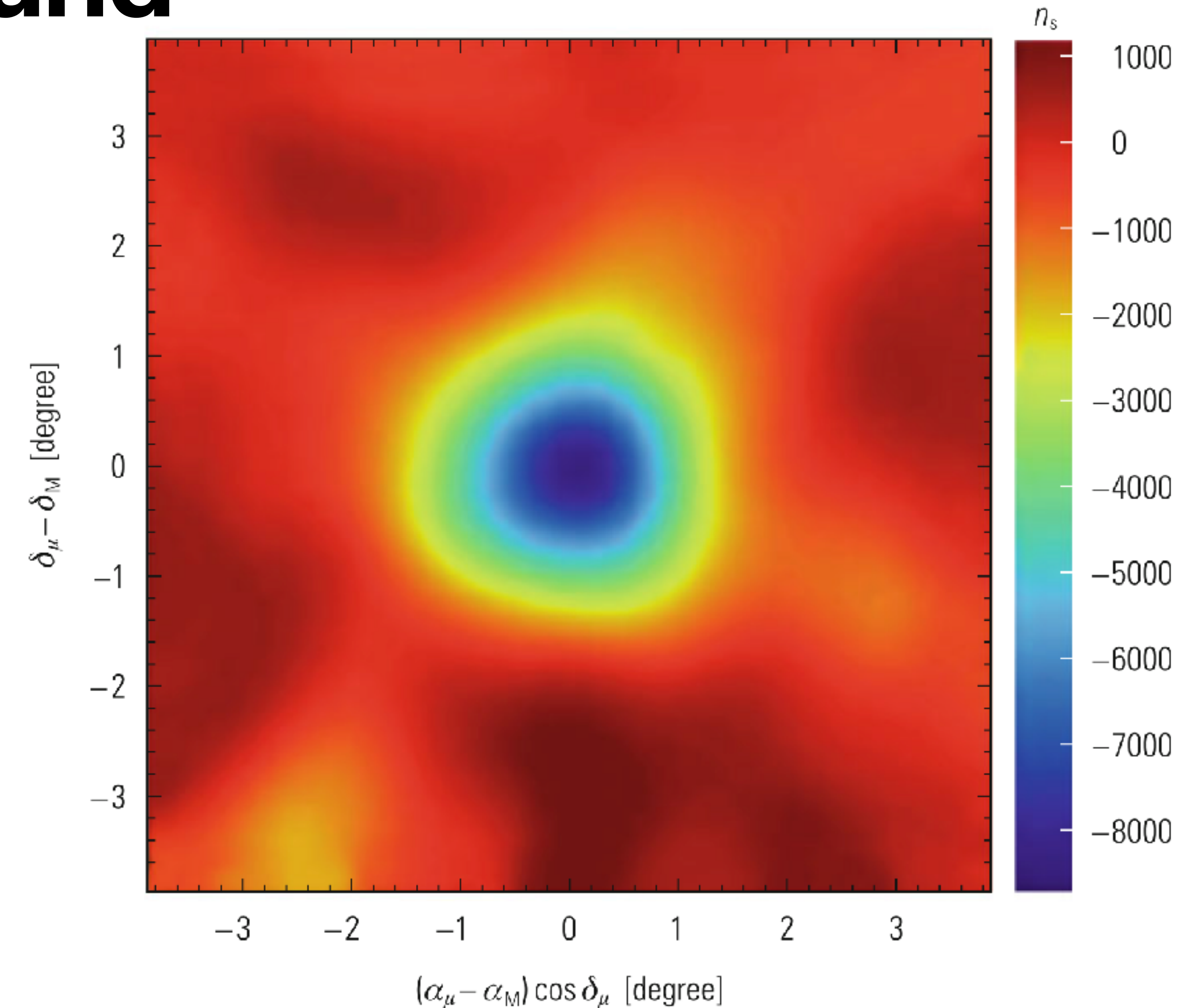


**Fig. 7.24** Contour plot of the muon deficit as measured by ICECUBE in the region around the Moon's position. Since ICECUBE only measures muons, this plot shows the image of the Moon by the absence of muons. The significance of the deficit is more than  $6\sigma$ . To obtain this map of the Moon shadow data from more than a year have been used [123]